

Tetranuclear Ni₄ cubane complexes with unexpectedly high χT maxima: magneto-structural analysis

Filip Torić^{a*}, Gordana Pavlović^b, Damir Pajić^a, Marina Cindrić^c, Krešo Zadro^a

^aDepartment of Physics, Faculty of Science, University of Zagreb, Croatia.

^bFaculty of Textile Technology, University of Zagreb

^cDepartment of Chemistry, Faculty of Science, University of Zagreb, Croatia.

† Footnotes relating to the title and/or authors should appear here.

Electronic Supplementary Information (ESI) available: [details of any supplementary information available should be included here]. See DOI: 10.1039/x0xx00000x

Table of content:

1. Additional information about fitting procedure and simulations
2. Table S1. Thermogravimetric data for seven tetranuclear Ni(II) complexes
3. Figure S1: Comparison of the PXRD patterns for prepared cubanes and calculated from the from the X-ray single-crystal structure.
4. Figure S2: Mercury-rendered labelled ORTEP view of the molecular structure of complex 2
5. Figure S3: Mercury-rendered labelled ORTEP view of the molecular structure of complex 3
6. Figure S4: Mercury-rendered labelled ORTEP view of the molecular structure of complex 4
7. Figure S5: Mercury-rendered labelled ORTEP view of the molecular structure of complex 5
8. Figure S6: Mercury-rendered labelled ORTEP view of the molecular structure of complex 6
9. Figure S7: Mercury-rendered labelled ORTEP view of the molecular structure of complex 7
10. Table S2: Bond distances around Ni (Å) in complexes 1 – 7
11. Table S3: Ni··Ni distances (Å) in complexes 1 – 7
12. Table S4: Bond angle values around Ni (°) in complexes 1 – 7
13. Table S5: Angle values Ni–O–Ni (°) in complexes 1 – 7
14. Table S6: Angle values (°) between planes O··Ni··O defined by the oxygen and nickel atoms of Ni₄O₄ cubane core in complexes 1 – 7
15. Table S7: Angle values (°) between plane O··Ni··O defined by the oxygen and nickel atoms of Ni₄O₄ cubane core and Ni··Ni vector in complexes 1 – 7
16. Table S8: Hydrogen bonding and contacts geometry (Å, °) for the clusters 1 – 7.
17. Figure S8: $\chi(T)$ and $\chi T(T)$ dependences for 1. Red line represents best-fitted curve.
18. Figure S9: Energy levels diagram for 1.
19. Figure S10: $\chi(T)$ and $\chi T(T)$ dependences for 2. Red line represents best-fitted curve.
20. Figure S11: Energy levels diagram for 2.
21. Figure S12: $\chi(T)$ and $\chi T(T)$ dependences for 3. Red line represents best-fitted curve.
22. Figure S13: Energy levels diagram for 3.
23. Figure S14: $\chi(T)$ and $\chi T(T)$ dependences for 4. Red line represents best-fitted curve.
24. Figure S15: Energy levels diagram for 4.
25. Figure S16: $\chi(T)$ and $\chi T(T)$ dependences for 5. Red line represents best-fitted curve.
26. Figure S17: Energy levels diagram for 5.
27. Figure S18: $\chi(T)$ and $\chi T(T)$ dependences for 6. Red line represents best-fitted curve.
28. Figure S19: Energy levels diagram for 6.
29. Figure S20: $\chi(T)$ and $\chi T(T)$ dependences for 7. Red line represents best-fitted curve.
30. Figure S21: Energy levels diagram for 7.

31. **Figure S22:** Simulation of contribution of intermolecular interactions to the χT
32. **Figure S23:** Simulation of contribution of the rhombic E ZFS parameter to the χT .
33. **Figure S24:** $M(H)$ curves for **1** measured at several temperatures
34. **Figure S25:** $M(H)$ curves for **2** measured at several temperatures
35. **Figure S26:** $M(H)$ curves for **3** measured at several temperatures
36. **Figure S27:** $M(H)$ curves for **4** measured at several temperatures
37. **Figure S28:** $M(H)$ curves for **5** measured at several temperatures
38. **Figure S29:** $M(H)$ curves for **6** measured at several temperatures
39. **Figure S30:** $M(H)$ curves for **7** measured at several temperatures
40. **Figure S31:** Hysteresis curve for **4** measured at 2K.
41. **Figure S32:** Dependence of zero-field splitting D to D_5 defined in text.
42. **Figure S33:** Dependence of zero-field splitting D to the average difference between longer and shorter bonds in the Ni octahedra.
43. **Figure S34:** Dependence of zero-field splitting D to the axial angle α_{axial} .

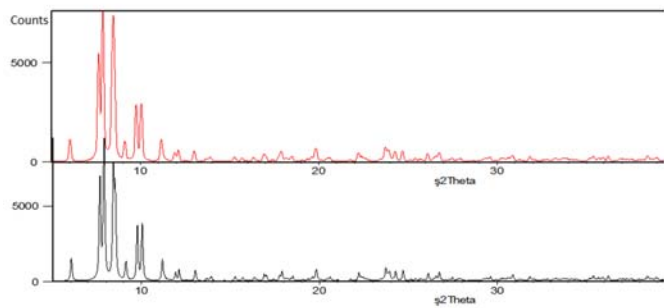
Additional information

It is important to point out that we were not able to reproduce magnetic behavior for all complexes by fitting to the model that includes only ZFS contribution, nor the intermolecular interactions. Due to the distorted octahedral environment of nickel ions we checked the influence of the rhombic ZFS contribution by plotting simulation curves and by trying fits. We could successfully fit data to the Hamiltonian including rhombic ZFS contribution and excluding intermolecular interaction (in this case single-ion D ZFS parameter is taken into account). Obtained fits have discrepancies from the data of one order higher than the discrepancies of the fits to the Hamiltonian in Eq. 4 and with high and unreasonable values of E ZFS parameter. Further simulations were performed fixing the values of the magnetic exchange interactions to $J_1 = -10 \text{ cm}^{-1}$, $J_2 = 20 \text{ cm}^{-1}$ and $g = 2.0$. Simulation of the influence of the intermolecular term is given in Fig. S22. From the Fig. S22 we can conclude that antiferromagnetic intermolecular interactions aren't responsible for the high χT maximum, but they influence the temperature of maximum in the way that z' increases the temperature of the maximum of χT . Ferromagnetic intermolecular interaction are also simulated. It shows that χT rapidly increases at low temperatures what is contrary to the measured χT which rapidly falls at low temperatures. Simulation of the rhombic ZFS contribution does not result in increasing the maximum of the χT curve (Figure S23). Therefore, high magnetic momenta come from the quadratic spin contribution contained in the axial ZFS term.

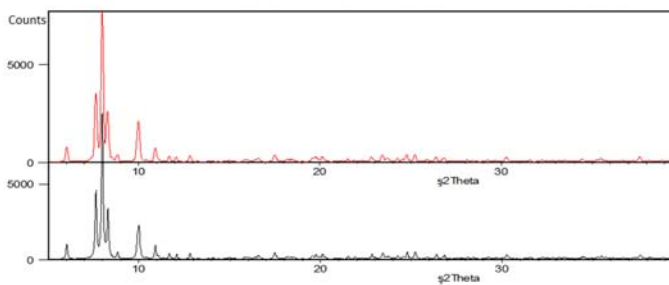
Table S1. Thermogravimetric data for seven tetranuclear Ni(II) complexes

	1 st step /°C	exp. w(ROH) (%)	calc. w(ROH)	2 nd /°C (pyrolysis)	exp. w(NiO) (%)	calc. w(NiO) (%)
1	115–183	17.23	17.47	313–398	21.65	21.71
2	110–189	20.36	20.70	317–437	21.23	21.47
3	100–192	23.51	23.69	292–394	20.54	20.66
4	120–245	21.95	22.22	306–413	22.01	21.90
5	144–207	15.66	15.75	307–450	21.33	21.47
6	154–232	17.09	17.47	278–415	20.72	20.66
7	84–269	17.62	17.47	301–402	22.37	22.81

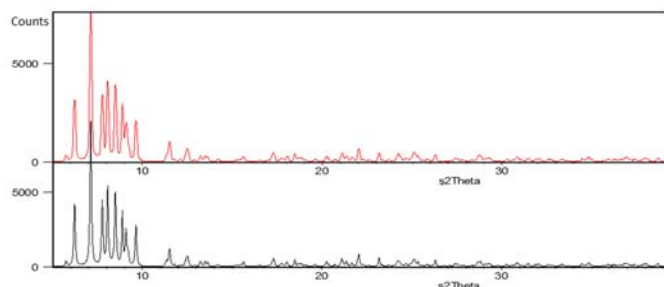
1



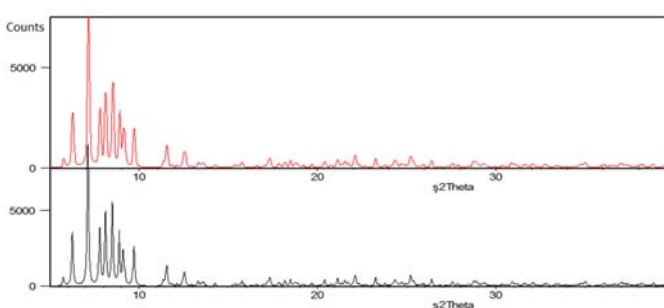
2



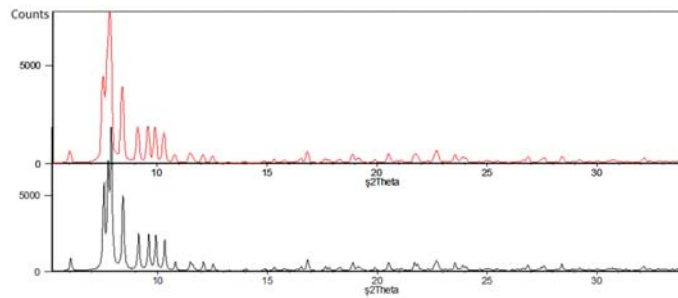
3



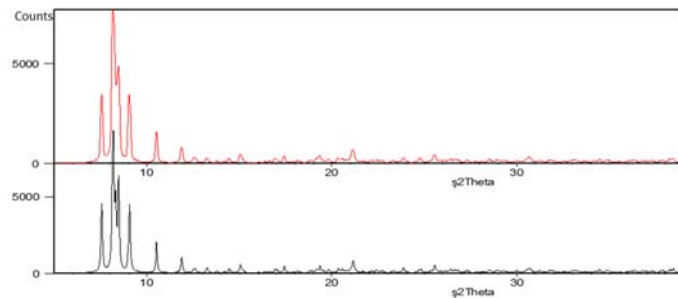
4



5



6



7

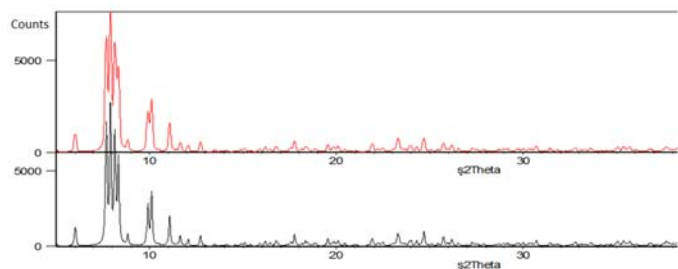


Figure S1: Comparison of the PXRD patterns for prepared cubanes (the red lines) and calculated from the X-ray single-crystal structure (the black lines).

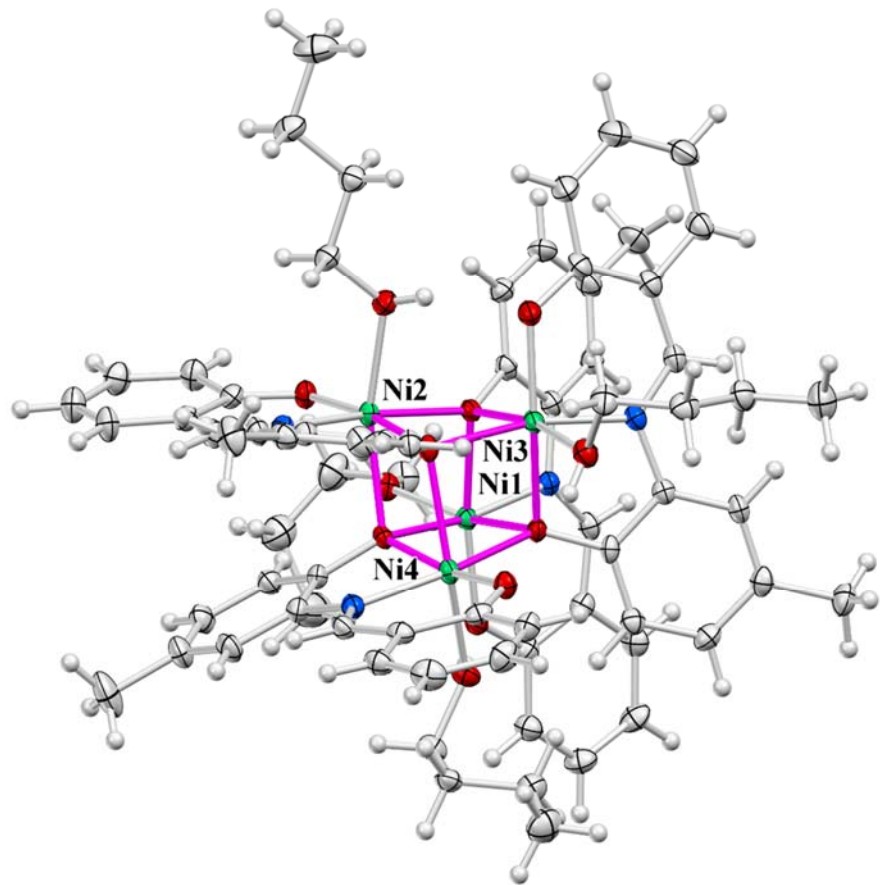


Figure S2: Mercury-rendered labelled ORTEP view of the molecular structure of complex **2** emphasizing the $\text{Ni}_4(\mu_3\text{-OR})_4$ moiety. Thermal ellipsoids are drawn with 50 % probability. Color scheme: Ni-green, O-red, N-blue, C-gray, H-light gray.

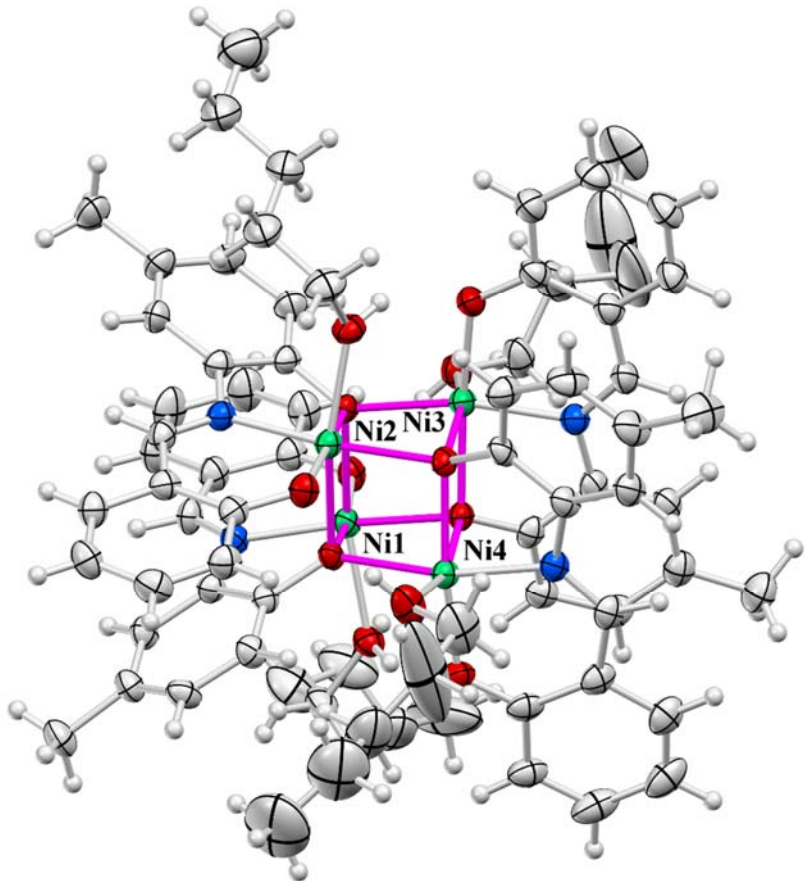


Figure S3: Mercury-rendered labelled ORTEP view of the molecular structure of complex **3** emphasizing the $\text{Ni}_4(\mu_3\text{-OR})_4$ moiety. Thermal ellipsoids are drawn with 50 % probability. The minor disordered component of alkyl ROH chain at Ni3 has been omitted. The H-atoms of alkyl ROH chain at Ni3 are not generated. Color scheme: Ni-green, O-red, N-blue, C-gray, H-light gray.

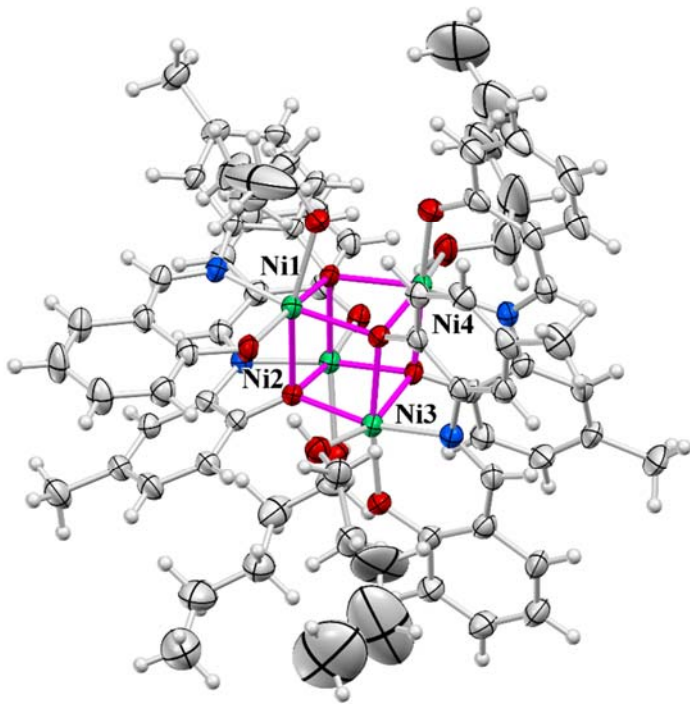


Figure S4: Mercury-rendered labelled ORTEP view of the molecular structure of complex **4** emphasizing the $\text{Ni}_4(\mu_3\text{-OR})_4$ moiety. Thermal ellipsoids are drawn with 50 % probability. The minor disordered component of alkyl ROH chain at Ni1 has been omitted. Color scheme: Ni-green, O-red, N-blue, C-gray, H-light gray.

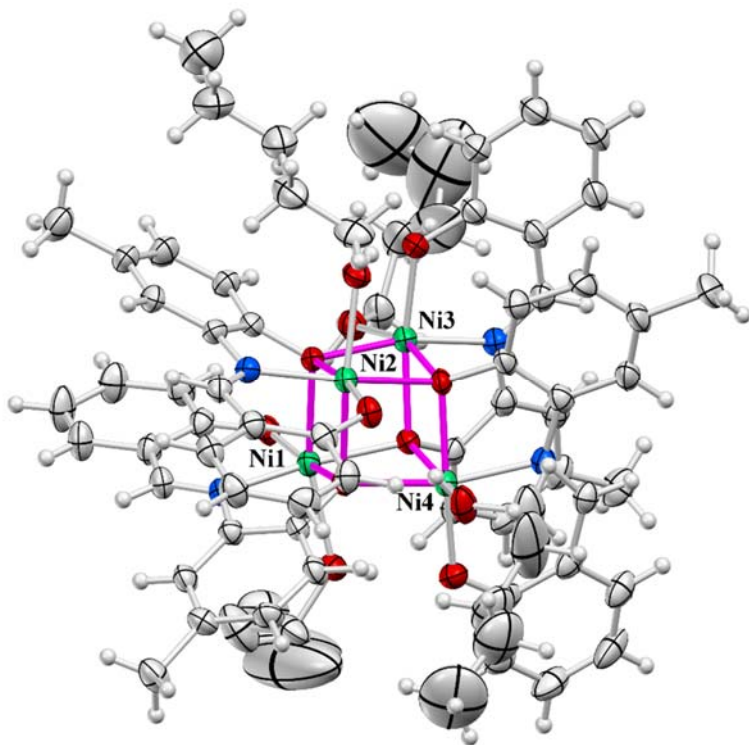


Figure S5: Mercury-rendered labelled ORTEP view of the molecular structure of complex 5 emphasizing the $\text{Ni}_4(\mu_3\text{-OR})_4$ moiety. Thermal ellipsoids are drawn with 50 % probability. The minor disordered component of alkyl ROH chain at Ni1 has been omitted. The H-atoms of alkyl ROH chain at Ni1 are not generated. Color scheme: Ni-green, O-red, N-blue, C-gray, H-light gray.

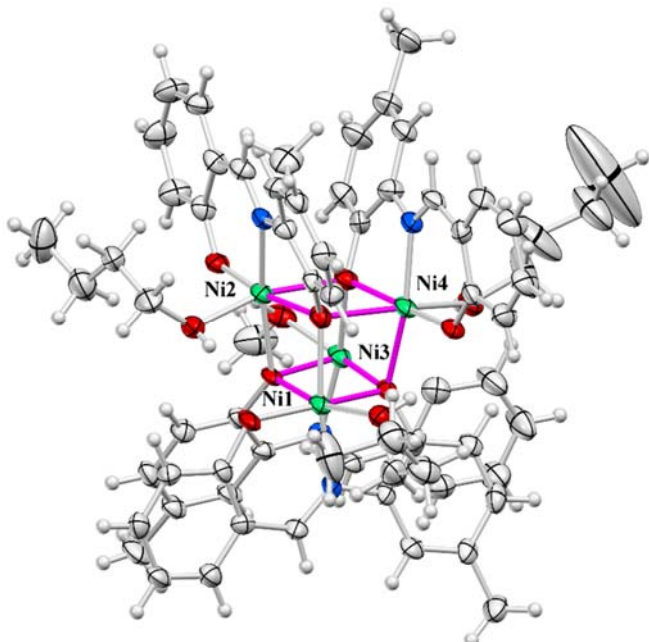


Figure S6: Mercury-rendered labelled ORTEP view of the molecular structure of complex 6 emphasizing the $\text{Ni}_4(\mu_3\text{-OR})_4$ moiety. Thermal ellipsoids are drawn with 50 % probability. Color scheme: Ni-green, O-red, N-blue, C-gray, H-light gray.

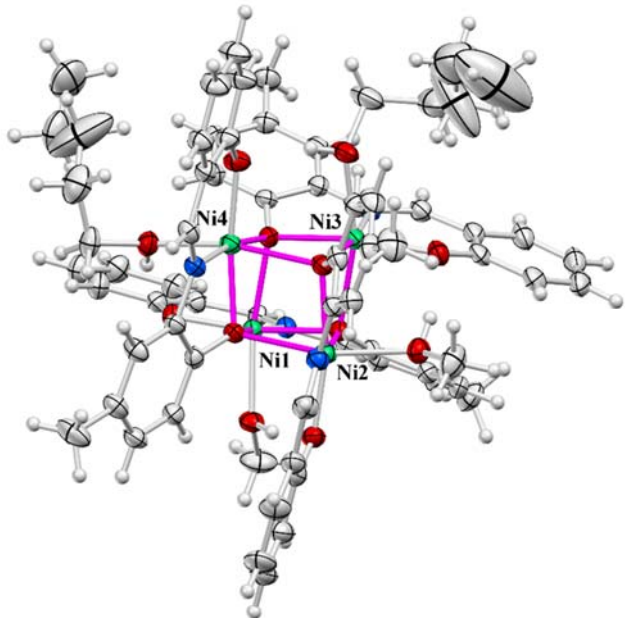


Figure S7: Mercury-rendered labelled ORTEP view of the molecular structure of complex 7 emphasizing the $\text{Ni}_4(\mu_3\text{-OR})_4$ moiety. Thermal ellipsoids are drawn with 50 % probability. The minor disordered component of two methylene groups of ROH chain at Ni4 has been omitted. Color scheme: Ni-green, O-red, N-blue, C-gray, H-light gray.

Table S2: Bond distances around Ni (\AA) in complexes **1 – 7**

	1	2	3	4	5	6	7
Ni1—O11	1.961(2)	1.955(2)	1.956(2)	1.952(2)	1.946(4)	1.960(2)	1.972(4)
Ni1—O12	2.056(2)	2.047(1)	2.059(2)	2.059(2)	2.042(4)	2.052(2)	2.057(4)
Ni1—O13	2.105(2)	2.110(2)	2.151(3)	2.145(3)	2.110(5)	2.099(2)	2.085(3)
Ni1—N11	1.974(2)	1.977(2)	1.972(3)	1.971(3)	1.960(6)	1.970(2)	1.976(4)
Ni1—O32	2.236(2)	2.236(2)	2.045(2)	2.046(2)	2.213(4)	2.207(2)	2.220(2)
Ni1—O42	1.975(2)	2.047(2)	1.986(3)	2.135(3)	2.093(4)	2.068(2)	2.082(4)
Ni2—O12	1.975(2)	2.060(2)	2.188(2)	2.192(3)	2.093(4)	2.046(2)	2.082(4)
Ni2—O21	1.962(2)	1.970(2)	1.964(2)	1.962(2)	1.948(4)	1.960(2)	1.950(3)
Ni2—O22	2.066(2)	2.067(2)	2.059(2)	2.059(2)	2.039(4)	2.068(2)	2.051(2)
Ni2—O23	2.112(2)	2.074(2)	2.093(3)	2.093(3)	2.111(4)	2.124(2)	2.103(4)
Ni2—N21	1.975(2)	1.977(2)	1.973(3)	1.976(3)	2.093(4)	1.959(2)	1.978(3)
Ni2—O42	2.232(2)	2.227(2)	2.037(2)	2.033(2)	2.203(4)	2.207(2)	2.221(3)
Ni3—O12	2.236(2)	2.192(2)	1.986(3)	2.135(3)	2.216(4)	2.206(2)	2.227(3)
Ni3—O22	1.975(2)	2.078(2)	2.048(2)	2.051(2)	2.093(4)	2.062(2)	2.082(4)
Ni3—O31	1.975(2)	1.972(2)	1.962(3)	1.964(3)	1.963(4)	1.974(2)	1.955(4)
Ni3—O32	2.078(2)	2.069(1)	2.064(3)	2.062(3)	2.066(4)	2.065(2)	2.040(3)
Ni3—O33	2.096(2)	2.100(2)	2.121(2)	2.117(2)	2.110(4)	2.103(2)	2.114(3)
Ni3—N31	1.970(2)	1.984(2)	1.976(3)	1.978(3)	2.093(4)	1.974(2)	1.977(5)
Ni4—O22	2.221(2)	2.266(2)	1.986(3)	2.135(3)	2.205(4)	2.234(2)	2.205(3)
Ni4—O32	1.975(2)	2.046(2)	2.238(2)	2.243(2)	2.093(4)	2.061(2)	2.082(4)
Ni4—O41	1.955(2)	1.957(2)	1.955(3)	1.965(3)	1.947(4)	1.955(2)	1.955(3)
Ni4—O42	2.052(1)	2.057(2)	2.039(3)	2.036(3)	2.067(4)	2.054(2)	2.058(2)
Ni4—O43	2.099(2)	2.128(2)	2.130(2)	2.135(3)	2.093(4)	2.114(2)	2.082(4)
Ni4—N41	1.975(2)	1.980(2)	1.986(3)	1.979(3)	1.972(6)	1.975(2)	1.972(5)

Table S3: Ni··Ni distances (\AA) in complexes **1 – 7**

	1	2	3	4	5	6	7
Ni1—Ni2	3.070	3.051	3.280	3.274	3.079	3.073	3.057
Ni1—Ni3	3.364	3.327	3.091	3.092	3.328	3.313	3.362
Ni1—Ni4	3.084	3.091	3.118	3.111	3.046	3.068	3.082
Ni2—Ni3	3.100	3.080	3.112	3.119	3.058	3.059	3.080
Ni2—Ni4	3.341	3.389	3.080	3.076	3.320	3.329	3.324
Ni3—Ni4	3.049	3.087	3.328	3.332	3.078	3.084	3.075

Table S4: Bond angle values ($^{\circ}$) in complexes **1 – 7**

	1	2	3	4	5	6	7
O11—Ni1—O12	169.91(8)	171.54(8)	169.24(9)	169.4(1)	171.3(2)	171.05(8)	171.4(1)
O11—Ni1—O13	100.57(8)	97.53(8)	102.8(1)	102.2(1)	97.3(2)	98.81(8)	98.7(1)
O11—Ni1—N11	94.16(9)	94.19(8)	93.9(1)	89.7(1)	88.0(2)	93.96(9)	89.6(1)
O11—Ni1—O32	93.44(7)	94.92(7)	97.95(9)	97.7(1)	94.1(2)	93.72(7)	96.4(1)
O11—Ni1—O42	90.35(8)	95.22(7)	92.6(1)	89.7(1)	88.0(2)	96.88(8)	89.6(1)
O12—Ni1—O13	89.22(7)	90.61(7)	87.59(9)	87.9(1)	91.1(2)	89.80(8)	89.3(1)
O12—Ni1—N11	82.87(8)	83.39(8)	82.7(1)	89.7(1)	88.0(2)	83.15(8)	89.6(1)
O12—Ni1—O32	77.29(7)	77.33(7)	85.56(9)	86.0(1)	77.8(2)	78.17(7)	76.1(1)
O12—Ni1—O42	90.35(8)	87.01(7)	92.6(1)	89.7(1)	88.0(2)	85.92(7)	89.6(1)
O13—Ni1—N11	92.28(8)	90.53(8)	91.5(1)	89.7(1)	88.0(2)	92.61(9)	89.6(1)
O13—Ni1—O32	163.60(7)	165.51(7)	86.09(9)	86.4(1)	166.2(2)	164.65(8)	163.3(1)
O13—Ni1—O42	90.35(8)	90.23(7)	92.6(1)	89.7(1)	88.0(2)	87.18(8)	89.6(1)
N11—Ni1—O32	95.19(8)	95.93(8)	168.1(1)	168.1(1)	96.6(2)	95.36(8)	93.1(1)
N11—Ni1—O42	90.35(8)	170.38(8)	92.6(1)	89.7(1)	88.0(2)	169.07(9)	89.6(1)
O32—Ni1—O42	90.35(8)	81.27(7)	92.6(1)	89.7(1)	88.0(2)	82.52(7)	89.6(1)
O12—Ni2—O21	90.35(8)	97.34(7)	92.52(9)	92.6(1)	88.0(2)	96.45(8)	89.6(1)
O12—Ni2—O22	90.35(8)	86.08(7)	80.13(9)	80.17(9)	88.0(2)	86.85(7)	89.6(1)
O12—Ni2—O23	90.35(8)	88.07(8)	163.60(9)	164.0(1)	88.0(2)	87.19(8)	89.6(1)
O12—Ni2—N21	90.35(8)	168.67(8)	98.4(1)	89.7(1)	88.0(2)	169.13(9)	89.6(1)
O12—Ni2—O42	90.35(8)	82.11(7)	81.93(9)	82.01(9)	88.0(2)	82.53(7)	89.6(1)
O21—Ni2—O22	169.78(8)	172.38(8)	171.2(1)	171.3(1)	169.6(2)	168.92(8)	171.8(1)
O21—Ni2—O23	100.48(8)	96.14(8)	101.8(1)	101.2(1)	100.4(2)	100.90(8)	97.4(1)
O21—Ni2—N21	94.50(8)	93.54(9)	94.1(1)	89.7(1)	88.0(2)	94.34(9)	89.6(1)
O21—Ni2—O42	93.52(7)	97.12(7)	97.26(9)	97.4(1)	92.5(2)	91.84(7)	95.0(1)
O22—Ni2—O23	89.11(8)	90.76(8)	86.15(9)	86.6(1)	89.8(2)	89.80(8)	90.5(1)
O22—Ni2—N21	82.31(8)	82.75(8)	82.3(1)	89.7(1)	88.0(2)	82.79(9)	89.6(1)
O22—Ni2—O42	77.25(7)	76.54(7)	86.60(9)	86.6(1)	77.8(2)	78.06(7)	77.5(1)
O23—Ni2—N21	87.39(8)	93.91(9)	88.5(1)	89.7(1)	88.0(2)	89.49(9)	89.6(1)
O23—Ni2—O42	165.25(7)	164.39(7)	88.37(9)	88.3(1)	164.2(2)	164.45(7)	165.4(1)
N21—Ni2—O42	96.19(8)	93.44(8)	168.6(1)	168.7(1)	88.0(2)	98.45(8)	95.9(1)
O12—Ni3—O22	90.35(8)	82.52(7)	92.6(1)	89.7(1)	88.0(2)	82.94(7)	89.6(1)
O12—Ni3—O31	95.45(7)	92.94(7)	92.6(1)	89.7(1)	93.9(2)	92.55(8)	93.6(1)
O12—Ni3—O32	76.86(7)	77.92(7)	92.6(1)	89.7(1)	77.2(2)	77.92(7)	76.3(1)
O12—Ni3—O33	164.14(7)	169.08(7)	92.6(1)	89.7(1)	165.4(2)	163.91(8)	162.5(1)
O12—Ni3—N31	92.98(8)	97.23(8)	92.6(1)	89.7(1)	88.0(2)	97.01(8)	89.6(1)
O22—Ni3—O31	90.35(8)	97.22(8)	97.5(1)	97.5(1)	88.0(2)	97.23(8)	89.6(1)
O22—Ni3—O32	90.35(8)	86.77(7)	85.88(9)	85.7(1)	88.0(2)	86.75(7)	89.6(1)
O22—Ni3—O33	90.35(8)	91.45(8)	87.7(1)	87.8(1)	88.0(2)	86.78(8)	89.6(1)
O22—Ni3—N31	90.35(8)	168.45(8)	167.6(1)	89.7(1)	88.0(2)	169.13(9)	89.6(1)
O31—Ni3—O32	170.92(8)	169.52(8)	168.4(1)	168.4(1)	170.0(2)	169.20(8)	169.1(1)
O31—Ni3—O33	98.79(8)	96.86(8)	102.3(1)	102.4(1)	98.4(2)	101.01(8)	101.0(1)

O31—Ni3—N31	93.39(8)	94.33(9)	94.3(1)	89.7(1)	88.0(2)	93.63(9)	89.6(1)
O32—Ni3—O33	89.48(7)	92.70(7)	88.90(9)	88.8(1)	91.0(2)	89.20(8)	89.6(1)
O32—Ni3—N31	82.34(8)	81.90(8)	81.8(1)	89.7(1)	88.0(2)	82.63(9)	89.6(1)
O33—Ni3—N31	93.12(9)	86.85(8)	93.6(1)	89.7(1)	88.0(2)	90.78(9)	89.6(1)
O22—Ni4—O32	90.35(8)	82.51(7)	92.6(1)	89.7(1)	88.0(2)	82.48(7)	89.6(1)
O22—Ni4—O41	93.94(8)	89.7(1)	92.6(1)	95.2(2)	93.7(1)	92.92(7)	94.73(7)
O22—Ni4—O42	77.72(7)	89.7(1)	92.6(1)	77.2(2)	77.7(1)	75.88(7)	77.77(7)
O22—Ni4—O43	163.94(8)	89.7(1)	92.6(1)	163.0(2)	165.2(1)	162.99(7)	166.10(7)
O22—Ni4—N41	94.70(8)	89.7(1)	92.6(1)	88.0(2)	89.6(1)	95.79(8)	96.79(8)
O32—Ni4—O41	95.44(8)	92.0(1)	91.95(9)	88.0(2)	89.6(1)	95.96(7)	90.35(8)
O32—Ni4—O42	86.58(7)	79.7(1)	79.65(9)	88.0(2)	89.6(1)	85.82(7)	90.35(8)
O32—Ni4—O43	87.92(8)	165.7(1)	164.8(1)	88.0(2)	89.6(1)	87.90(7)	90.35(8)
O32—Ni4—N41	169.62(9)	89.7(1)	96.0(1)	88.0(2)	89.6(1)	169.18(8)	90.35(8)
O41—Ni4—O42	171.12(8)	170.4(1)	170.1(1)	171.3(2)	170.2(1)	168.36(8)	171.88(7)
O41—Ni4—O43	99.77(8)	99.2(1)	100.0(1)	100.1(2)	99.5(1)	102.06(8)	96.57(8)
O41—Ni4—N41	94.71(9)	89.7(1)	94.0(1)	88.0(2)	89.6(1)	94.80(9)	94.62(8)
O42—Ni4—O43	88.93(8)	89.7(1)	89.2(1)	88.0(2)	89.6(1)	89.48(7)	91.30(8)
O42—Ni4—N41	83.06(8)	89.7(1)	81.8(1)	88.0(2)	89.6(1)	83.40(8)	83.32(8)
O43—Ni4—N41	92.47(9)	89.7(1)	92.6(1)	88.0(2)	89.6(1)	91.00(9)	90.35(8)

Table S5: Angle values Ni–O–Ni ($^{\circ}$) in complexes **1 – 7**

	1	2	3	4	5	6	7						
Ni1-O22-Ni2	96.31(7)	Ni1-O12-Ni2	95.94(7)	Ni1-O12-Ni2	101.07(9)	Ni1-O12-Ni2	100.66(10)	Ni1-O22-Ni2	97.68(18)	Ni1-O12-Ni2	97.14(8)	Ni1-O22-Ni2	96.01(12)
Ni1-O32-Ni2	91.00(7)	Ni1-O42-Ni2	90.99(7)	Ni1-O22-Ni2	99.66(9)	Ni1-O22-Ni2	99.71(10)	Ni1-O32-Ni2	92.27(16)	Ni1-O42-Ni2	91.83(7)	Ni1-O32-Ni2	91.02(11)
Ni1-O12-Ni3	103.19(7)	Ni1-O12-Ni3	103.38(7)	Ni1-O22-Ni3	92.42(8)	Ni1-O22-Ni3	92.60(10)	Ni1-O12-Ni3	102.74(16)	Ni1-O12-Ni3	102.13(7)	Ni1-O12-Ni3	103.33(13)
Ni1-O32-Ni3	102.46(7)	Ni1-O32-Ni3	101.16(7)	Ni1-O32-Ni3	97.57(9)	Ni1-O32-Ni3	97.62(11)	Ni1-O32-Ni3	102.03(16)	Ni1-O32-Ni3	101.66(7)	Ni1-O32-Ni3	104.13(13)
Ni2-O32-Ni3	96.93(7)	Ni2-O12-Ni3	92.78(7)	Ni2-O22-Ni3	98.51(9)	Ni2-O22-Ni3	98.75(10)	Ni2-O32-Ni3	95.85(15)	Ni2-O12-Ni3	91.95(7)	Ni2-O32-Ni3	97.33(12)
Ni2-O42-Ni3	92.64(7)	Ni2-O22-Ni3	95.98(7)	Ni2-O42-Ni3	92.20(8)	Ni2-O42-Ni3	92.31(9)	Ni2-O42-Ni3	92.02(15)	Ni2-O22-Ni3	95.59(8)	Ni2-O42-Ni3	92.01(11)
Ni1-O12-Ni4	97.58(7)	Ni1-O32-Ni4	92.31(6)	Ni1-O12-Ni4	98.34(9)	Ni1-O12-Ni4	98.03(10)	Ni1-O12-Ni4	96.21(16)	Ni1-O32-Ni4	91.85(7)	Ni1-O12-Ni4	97.13(12)
Ni1-O22-Ni4	92.25(6)	Ni1-O42-Ni4	97.76(7)	Ni1-O32-Ni4	93.31(9)	Ni1-O32-Ni4	92.86(10)	Ni1-O22-Ni4	91.32(15)	Ni1-O42-Ni4	96.19(8)	Ni1-O22-Ni4	92.38(11)
Ni2-O22-Ni4	102.35(7)	Ni2-O22-Ni4	102.81(7)	Ni2-O12-Ni4	92.81(8)	Ni2-O12-Ni4	92.56(9)	Ni2-O22-Ni4	102.84(18)	Ni2-O22-Ni4	101.32(7)	Ni2-O22-Ni4	102.66(11)
Ni2-O42-Ni4	102.42(7)	Ni2-O42-Ni4	104.50(7)	Ni2-O42-Ni4	98.14(9)	Ni2-O42-Ni4	98.21(10)	Ni2-O42-Ni4	102.02(17)	Ni2-O42-Ni4	102.72(7)	Ni2-O42-Ni4	101.91(11)
Ni3-O12-Ni4	90.76(6)	Ni3-O22-Ni4	90.49(6)	Ni3-O32-Ni4	101.27(9)	Ni3-O32-Ni4	101.32(10)	Ni3-O12-Ni4	92.23(14)	Ni3-O22-Ni4	91.68(7)	Ni3-O12-Ni4	91.72(12)
Ni3-O42-Ni4	95.98(7)	Ni3-O32-Ni4	97.23(7)	Ni3-O42-Ni4	100.79(9)	Ni3-O42-Ni4	100.75(10)	Ni3-O42-Ni4	96.93(15)	Ni3-O32-Ni4	96.75(8)	Ni3-O42-Ni4	96.70(13)

Table S6: Angle values between planes O–Ni–O defined by the oxygen and nickel atoms of Ni_4O_4 cubane core in complexes **1 – 7**

	1	2	3	4	5	6	7						
Ni1··O22··O32··Ni2	161.27	Ni1··O12··O42··Ni2	159.58	Ni1··O12··O22··Ni2	179.43	Ni1··O12··O22··Ni2	179.52	Ni1··O22··O32··Ni2	164.28	Ni1··O12··O42··Ni2	163.58	Ni1··O22··O32··Ni2	160.44
Ni1··O12··O32··Ni3	175.68	Ni1··O12··O32··Ni3	175.67	Ni1··O22··O32··Ni3	164.21	Ni1··O22··O32··Ni3	164.32	Ni1··O12··O32··Ni3	176.02	Ni1··O12··O32··Ni3	176.84	Ni1··O12··O32··Ni3	175.83
Ni1··O12··O22··Ni4	164.14	Ni1··O32··O42··Ni4	162.94	Ni1··O12··O32··Ni4	165.36	Ni1··O12··O32··Ni4	165.61	Ni1··O12··O22··Ni4	161.27	Ni1··O32··O42··Ni4	162.65	Ni1··O12··O22··Ni4	163.01
Ni2··O32··O42··Ni3	163.84	Ni2··O12··O22··Ni3	163.34	Ni2··O22··O42··Ni3	166.23	Ni2··O22··O42··Ni3	166.02	Ni2··O32··O42··Ni3	162.31	Ni2··O12··O22··Ni3	163.24	Ni2··O32··O42··Ni3	162.87
Ni2··O22··O42··Ni4	175.62	Ni2··O22··O42··Ni4	175.06	Ni2··O12··O42··Ni4	165.43	Ni2··O12··O42··Ni4	165.72	Ni2··O22··O42··Ni4	176.56	Ni2··O22··O42··Ni4	175.86	Ni2··O22··O42··Ni4	175.49
Ni3··O12··O42··Ni4	160.69	Ni3··O22··O32··Ni4	162.20	Ni3··O32··O42··Ni4	178.74	Ni3··O32··O42··Ni4	178.68	Ni3··O12··O42··Ni4	163.5	Ni3··O22··O32··Ni4	164.31	Ni3··O12··O42··Ni4	161.81

Table S7: Angle values ($^{\circ}$) between plane O-Ni-O defined by the oxygen and nickel atoms of Ni_4O_4 cubane core and Ni-Ni vector in complexes **1 - 7**

Angle	1	Angle	2	Angle	3	Angle	4	Angle	5	Angle	6	Angle	7
Ni1·O22··Ni2··O32	9.67	Ni1··O12··Ni2··O42	9.77	Ni1··O12··Ni2··O22	0.28	Ni1··O12··Ni2··O22	0.24	Ni1··O22··Ni2··O32	8.13	Ni1··O12··Ni2··O42	7.97	Ni1··O22··Ni2··O32	10.12
Ni1··O12··Ni3··O32	2.13	Ni1··O12··Ni3··O32	2.16	Ni1··O22··Ni3··O32	8.15	Ni1··O22··Ni3··O32	8.08	Ni1··O12··Ni3··O32	1.96	Ni1··O12··Ni3··O32	1.57	Ni1··O12··Ni3··O32	2.08
Ni1··O12··Ni4··O22	7.66	Ni1··O32··Ni4··O42	8.84	Ni1··O12··Ni4··O32	7.01	Ni1··O12··Ni4··O32	6.88	Ni1··O12··Ni4··O22	9.02	Ni1··O32··Ni4··O42	8.96	Ni1··O12··Ni4··O22	8.23
Ni2··O22··Ni1··O32	9.03	Ni2··O12··Ni1··O42	10.62	Ni2··O12··Ni1··O22	0.28	Ni2··O12··Ni1··O22	0.23	Ni2··O22··Ni1··O32	7.56	Ni2··O12··Ni1··O42	8.43	Ni2··O22··Ni1··O32	9.41
Ni2··O32··Ni3··O42	8.35	Ni2··O12··Ni3··O22	8.06	Ni2··O22··Ni3··O42	6.54	Ni2··O22··Ni3··O42	6.62	Ni2··O32··Ni3··O42	9.11	Ni2··O12··Ni3··O22	8.09	Ni2··O32··Ni3··O42	8.89
Ni2··O22··Ni4··O42	2.19	Ni2··O22··Ni4··O42	2.44	Ni2··O12··Ni4··O42	7.46	Ni2··O12··Ni4··O42	7.32	Ni2··O22··Ni4··O42	1.70	Ni2··O22··Ni4··O42	2.05	Ni2··O22··Ni4··O42	2.24
Ni3··O12··Ni1··O32	2.15	Ni3··O12··Ni1··O32	2.15	Ni3··O22··Ni1··O32	7.61	Ni3··O22··Ni1··O32	7.57	Ni3··O12··Ni1··O32	1.99	Ni3··O12··Ni1··O32	1.57	Ni3··O12··Ni1··O32	2.07
Ni3··O32··Ni2··O42	7.78	Ni3··O12··Ni2··O22	8.57	Ni3··O22··Ni2··O42	7.19	Ni3··O22··Ni2··O42	7.33	Ni3··O32··Ni2··O42	8.55	Ni3··O12··Ni2··O22	8.65	Ni3··O32··Ni2··O42	8.22
Ni3··O12··Ni4··O42	10.03	Ni3··O22··Ni4··O32	8.58	Ni3··O32··Ni4··O42	0.63	Ni3··O32··Ni4··O42	0.66	Ni3··O12··Ni4··O42	8.49	Ni3··O22··Ni4··O32	7.55	Ni3··O12··Ni4··O42	9.42
Ni4··O12··Ni1··O22	8.18	Ni4··O32··Ni1··O42	8.20	Ni4··O12··Ni1··O32	7.61	Ni4··O12··Ni1··O32	7.48	Ni4··O12··Ni1··O22	9.68	Ni4··O32··Ni1··O42	8.36	Ni4··O12··Ni1··O22	8.73
Ni4··O22··Ni2··O42	2.17	Ni4··O22··Ni2··O42	2.46	Ni4··O12··Ni2··O42	7.08	Ni4··O12··Ni2··O42	6.94	Ni4··O22··Ni2··O42	1.72	Ni4··O22··Ni2··O42	2.06	Ni4··O22··Ni2··O42	2.24
Ni4··O12··Ni3··O42	9.24	Ni4··O22··Ni3··O32	9.19	Ni4··O32··Ni3··O42	0.61	Ni4··O32··Ni3··O42	0.64	Ni4··O12··Ni3··O42	7.99	Ni4··O22··Ni3··O32	8.11	Ni4··O12··Ni3··O42	8.74

Table S8: Hydrogen bonding and contacts geometry (\AA , $^\circ$) for the clusters **1–7**.

D–H···A	D–H	H···A	D···A	\angle D–H···A	Symmetry code
1					
O13–H13O···O41	0.84(2)	1.84(2)	2.655(3)	165(1)	-
O23–H23O···O11	0.84(2)	1.87(2)	2.673(2)	161(2)	-
O33–H33O···O21	0.83(3)	1.98(3)	2.712(3)	146(3)	-
O43–H43O···O31	0.83(2)	1.88(2)	2.685(3)	162(2)	-
C110–H110···O43	0.95	2.45	3.214(3)	137	-
C210–H210···O13	0.95	2.43	3.184(3)	136	-
C310–H310···O23	0.95	2.69	3.438(4)	136	-
C410–H410···O33	0.95	2.50	3.255(3)	136	-
C116–H11F···N11	0.99	2.90	3.577(4)	126	-
C117–H11H···O11	0.98	2.70	3.491(4)	138	-
C217–H21H···N21	0.98	2.99	3.675(6)	128	-
C415–H41F···N41	0.99	2.50	3.149(5)	123	-
C41B–H41N···O41	0.99	3.00	3.720(19)	131	-
2					
O13–H13O···O21	0.83(2)	1.87(2)	2.680(3)	163(2)	-
O23–H23O···O31	0.83(3)	1.93(3)	2.701(3)	152(2)	-
O33–H33O···O41	0.83(2)	2.00(2)	2.770(2)	154(2)	-
O43–H43O···O11	0.83(2)	1.84(2)	2.653(3)	166(1)	-
C110–H110···O23	0.95	2.47	3.218(3)	136	-
C210–H210···O33	0.95	2.67	3.421(4)	136	-
C310–H310···O43	0.95	2.41	3.176(3)	137	-
C410–H410···O13	0.95	2.47	3.240(3)	138	-
C315–H31E···O31	0.99	2.54	3.222(4)	126	-
C317–H31I···N31	0.99	2.96	3.609(4)	124	-
C416–H41G···N41	0.99	2.87	3.554(4)	127	-
C417–H41I···O41	0.99	2.98	3.750(3)	135	-
C118–H11K···O11	0.98	2.89	3.852(4)	169	$-x+2, -y, -z$
3					
O13–H13O···O41	0.84(6)	1.89(6)	2.686(3)	159(6)	-
O23–H23O···O31	0.84(5)	1.95(7)	2.692(3)	147(5)	-
O33–H33O···O11	0.84(6)	1.83(6)	2.660(3)	169(5)	-
O43–H43O···O21	0.84(5)	1.92(6)	2.722(4)	158(4)	-
C110–H110···O43	0.95	2.41	3.180(4)	139	-
C210–H210···O33	0.95	2.42	3.180(5)	136	-
C310–H310···O13	0.95	2.42	3.165(4)	135	-
C410–H410···O23	0.95	2.48	3.214(5)	134	-
C116–H11F···N11	0.99	2.84	3.537(7)	128	-
C117–H11I···O11	0.99	2.96	3.720(7)	134	-
4					
O13–H13O···O41	0.83(4)	1.87(3)	2.690(4)	172(3)	-

O23–H23O…O31	0.85(4)	1.92(4)	2.702(4)	153(4)	-
O33–H33O…O11	0.83(4)	1.85(4)	2.661(4)	163(3)	-
O43–H43O…O21	0.84(4)	1.92(4)	2.755(5)	174(3)	-
C110–H110…O43	0.95	2.39	3.172(5)	139	-
C210–H210…O33	0.95	2.42	3.176(5)	137	-
C313–H313…O13	0.95	2.44	3.182(5)	134	-
C413–H413…O23	0.95	2.47	3.203(5)	134	-

5

O23–H23O…O11	0.84(1)	1.96(16)	2.662(5)	140(22)	-
O33–H33O…O21	0.84(1)	1.81(5)	2.635(6)	168(24)	-
O43–H43O…O31	0.84(1)	1.92(15)	2.648(7)	144(23)	-
O13–H13O…O41	0.84(1)	1.92(11)	2.688(6)	151(22)	-
C112–H112…O43	0.95	2.52	3.268(7)	136	-
C210–H210…O13	0.95	2.45	3.216(7)	138	-
C310–H310…O23	0.95	2.43	3.187(8)	137	-
C410–H410…O33	0.95	2.48	3.235(8)	137	-
C216–21F…N22	0.99	2.82	3.528(9)	129	-
C217–H21I…O21	0.99	2.68	3.459(9)	136	-
C118–H11K…O11	0.98	2.94	3.905(11)	171	$-x+1, -y+1, -z+1$

6

O13–H13O…O21	0.84(3)	1.79(4)	2.614(3)	167(3)	-
O33–H33O…O41	0.84(6)	1.83(5)	2.650(3)	165(5)	-
O43–H43O…O11	0.84(4)	1.83(4)	2.619(3)	158(4)	-
O23–H23O…O31	0.84(5)	1.80(5)	2.615(3)	163(5)	-
C110–H110…O23	0.95	2.45	3.195(3)	136	-
C210–H210…O33	0.95	2.46	3.207(4)	135	-
C310–H310…O43	0.95	2.47	3.228(3)	137	-
C410–H410…O13	0.95	2.48	3.231(4)	136	-
C31A–H31D…O31	0.99	2.62	3.421(10)	138	-
C114–H11B…O23	0.98	2.73	3.660(4)	159	$-x+1, -y+1, -z+1$
C114–H11B…O21	0.98	2.65	3.342(4)	128	$-x+1, -y+1, -z+1$
C25–H25…O11	0.95	2.62	3.422(4)	143	$x, -y+1/2+1, +z-1/2$

7

O13–H13O…O41	0.83(2)	1.87(5)	2.675(5)	163(14)	-
O23–H23O…O11	0.83(2)	2.10(11)	2.689(5)	128(12)	-
O33–H33O…O21	0.84(2)	1.82(5)	2.625(4)	160(13)	-
O43–H43O…O31	0.84(2)	1.86(6)	2.643(5)	156(14)	-
C110–H110…O43	0.95	2.57	3.309(6)	135	-
C210–H210…O13	0.95	2.51	3.259(6)	136	-

C310– H310···O23	0.95	2.49	3.252(6)	138	-
C410– H410···O33	0.95	2.41	3.170(6)	137	-
C115– H11E···N11	0.99	2.65	3.277(8)	121	-

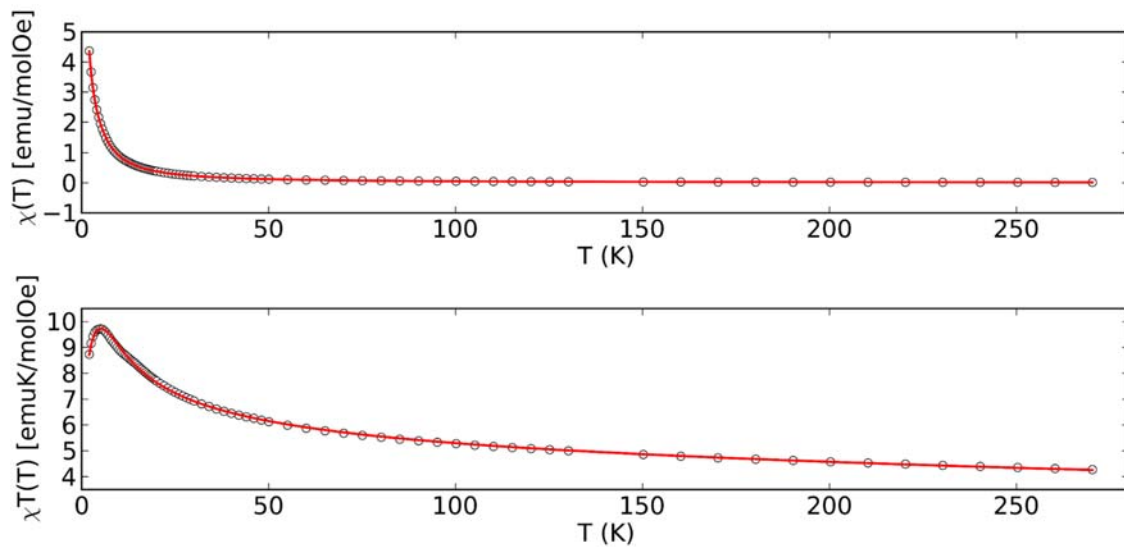


Figure S8: $\chi(T)$ and $\chi T(T)$ dependences for **1**. Red line represents best-fitted curve.

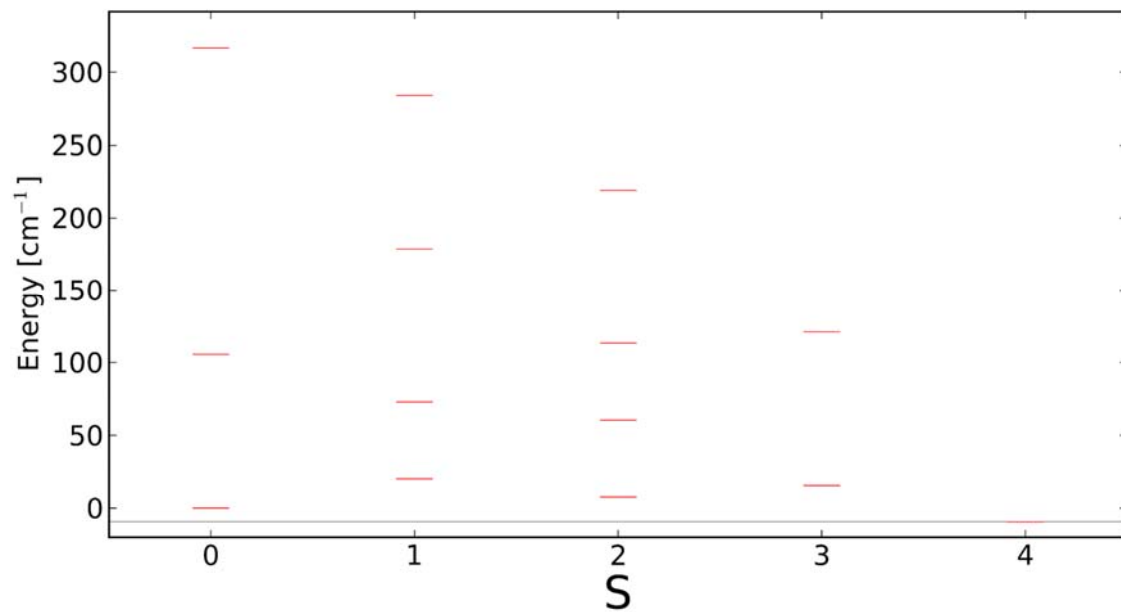


Figure S9: Energy levels diagram for **1**.

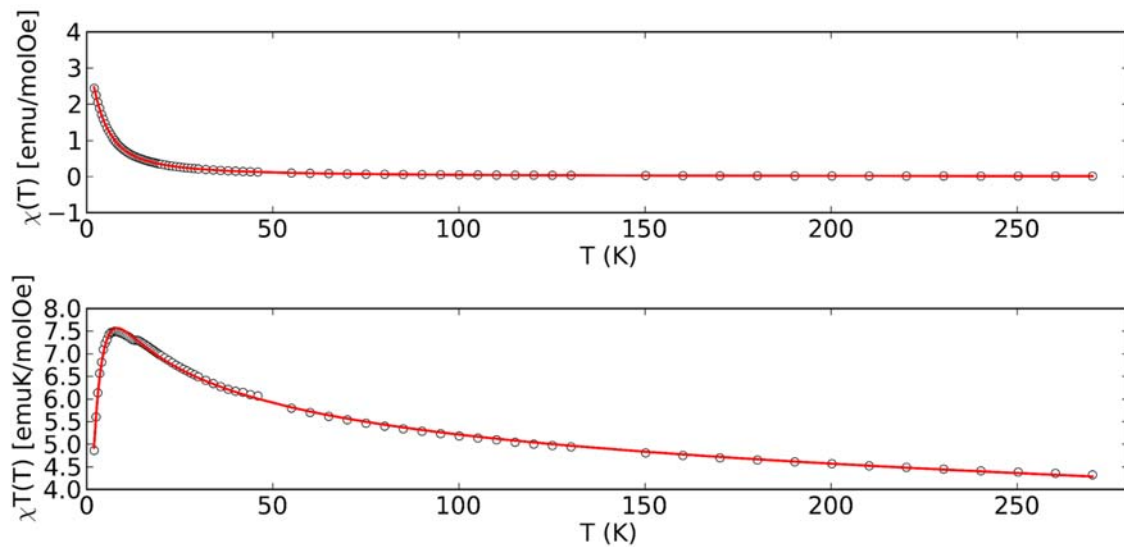


Figure S10: $\chi(T)$ and $\chi T(T)$ dependences for **2**. Red line represents best-fitted curve.

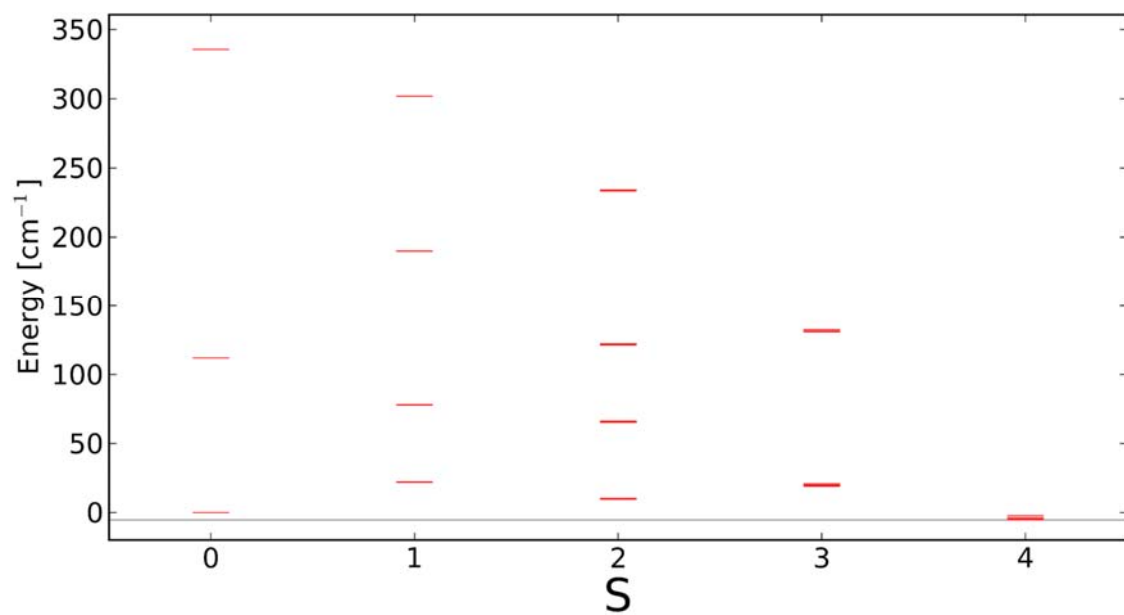


Figure S11: Energy levels diagram for **2**.

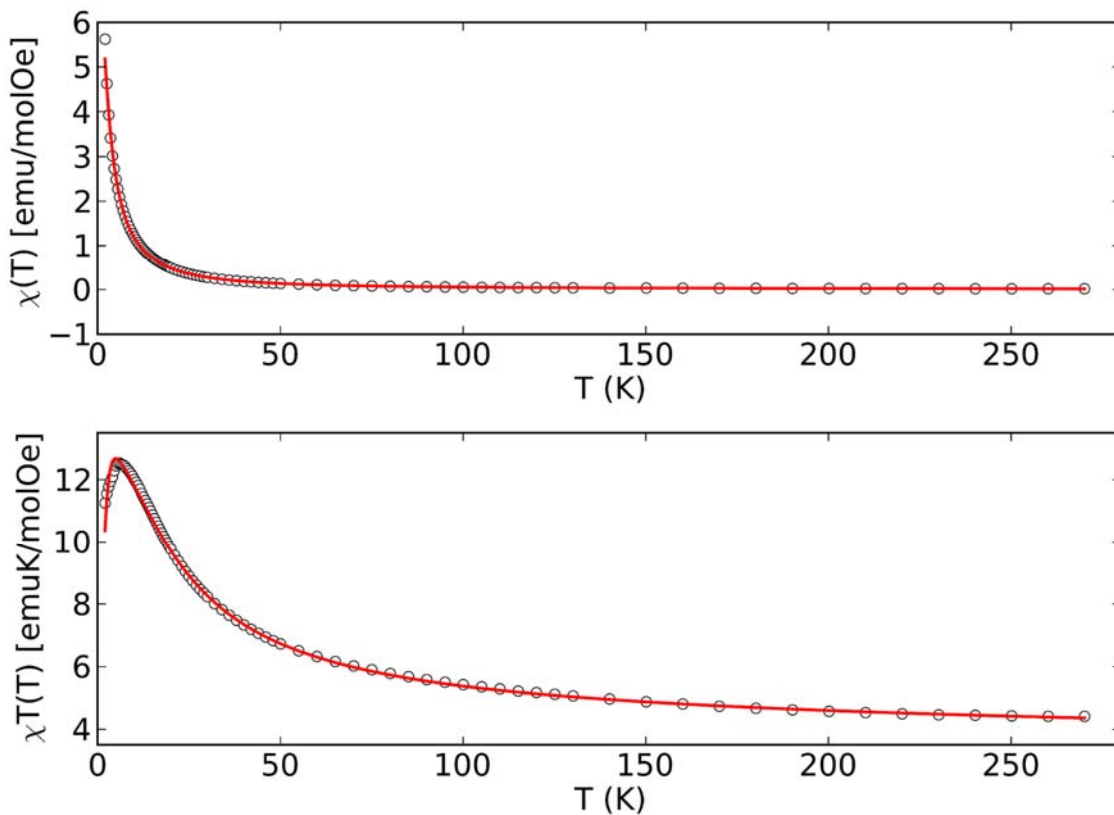


Figure S12: $\chi(T)$ and $\chi T(T)$ dependences for **3**. Red line represents best-fitted curve.

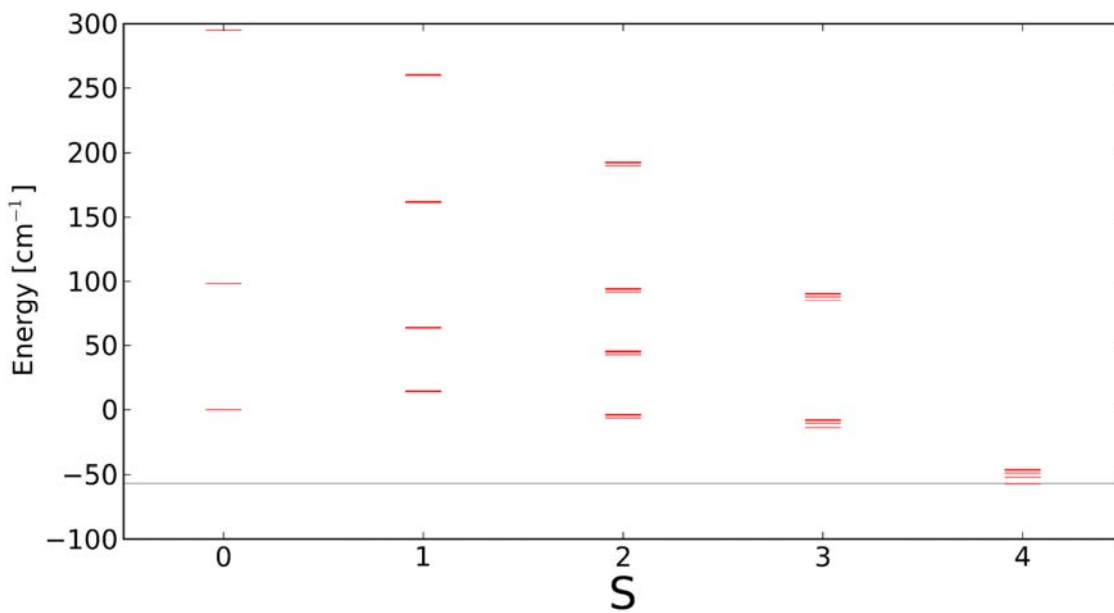


Figure S13: Energy levels diagram for **3**.

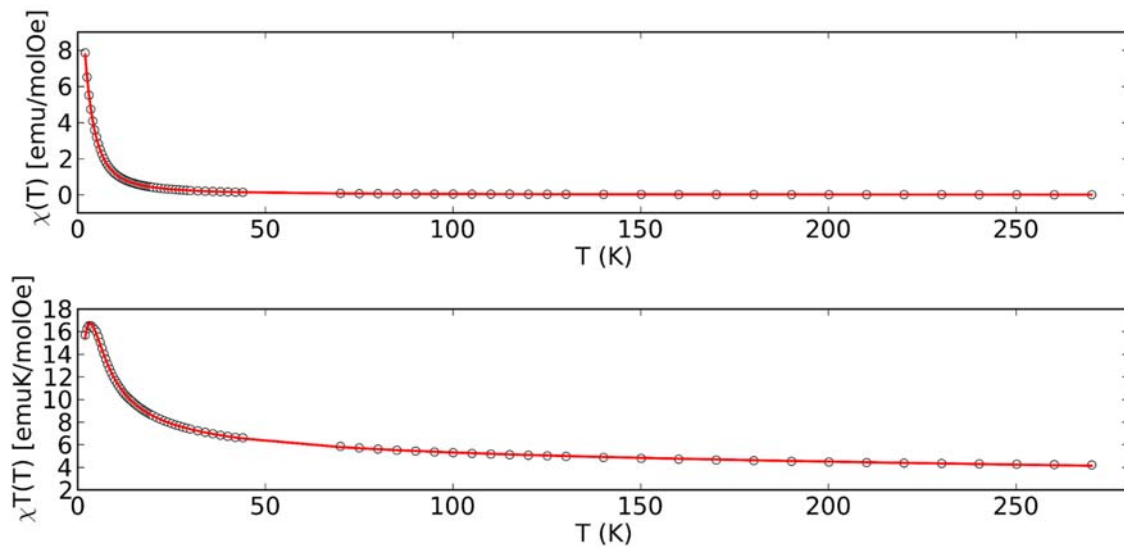


Figure S14: $\chi(T)$ and $\chi T(T)$ dependences for **4**. Red line represents best-fitted curve.

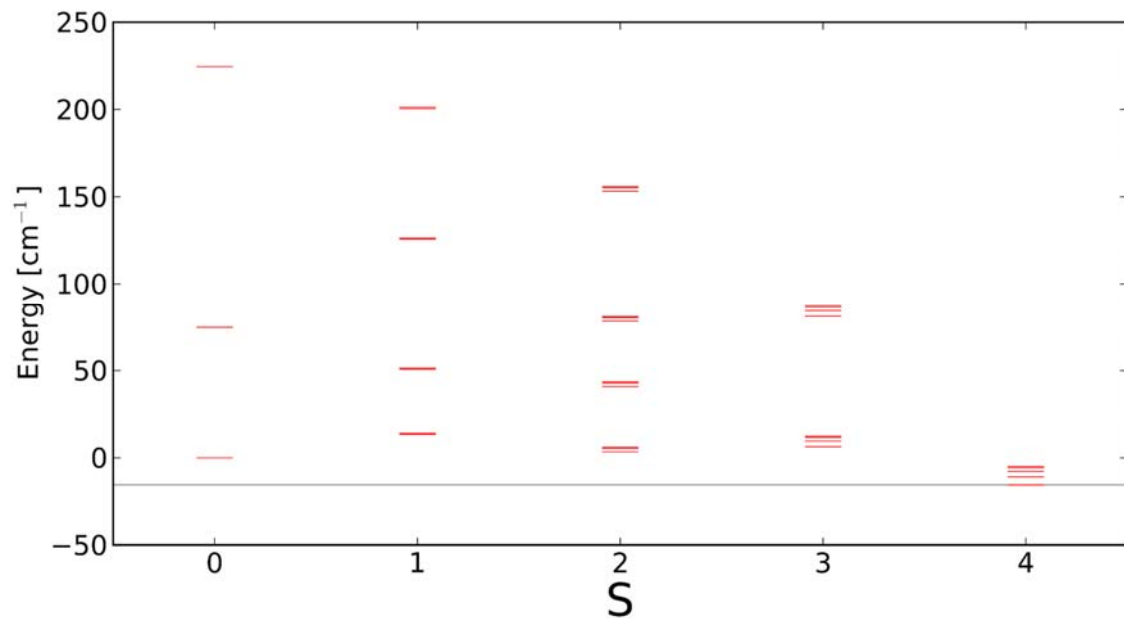


Figure S15: Energy levels diagram for **4**.

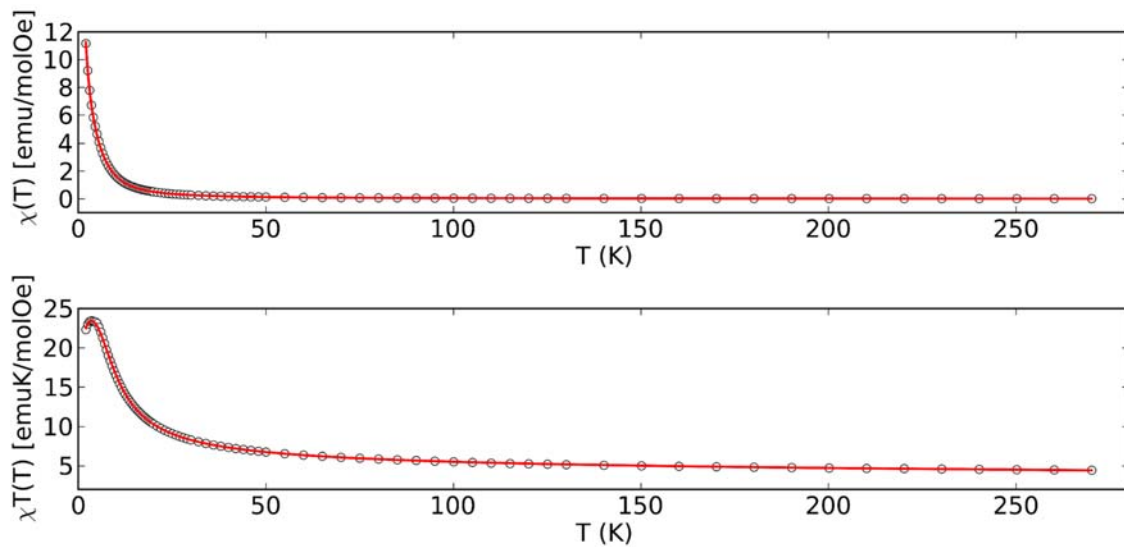


Figure S16: $\chi(T)$ and $\chi T(T)$ dependences for **5**. Red line represents best-fitted curve.

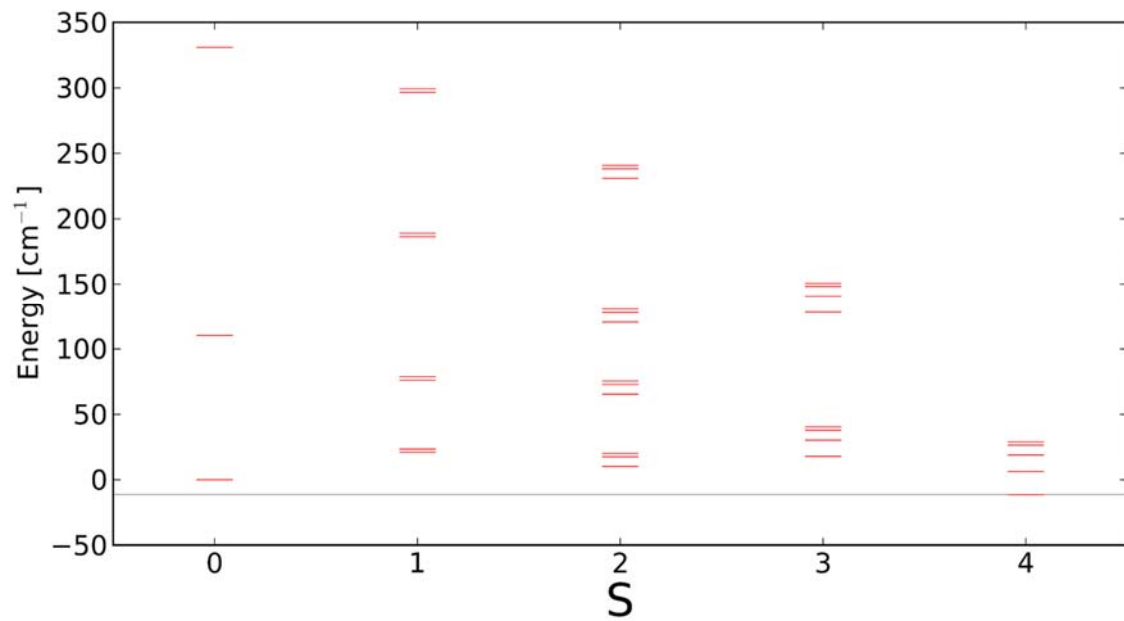


Figure S17: Energy levels diagram for **5**.

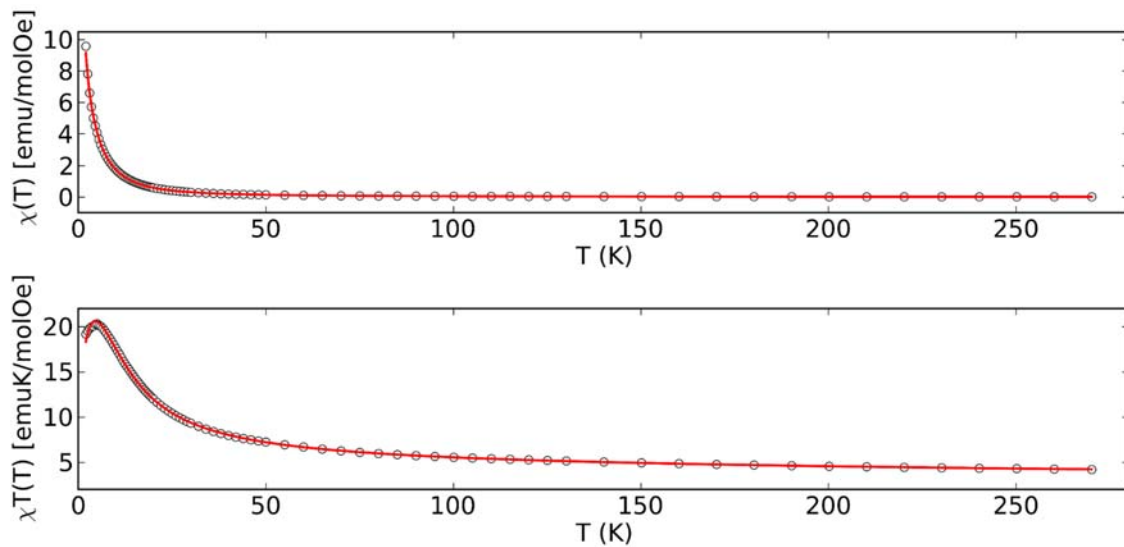


Figure S18: $\chi(T)$ and $\chi T(T)$ dependences for **6**. Red line represents best-fitted curve.

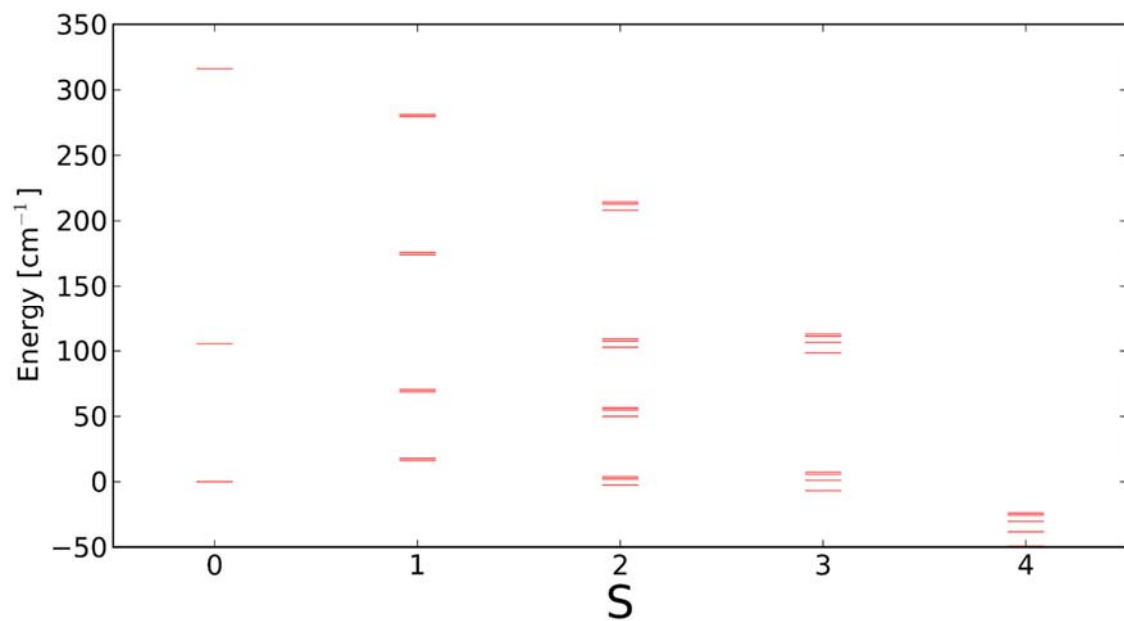


Figure S19: Energy levels diagram for **6**.

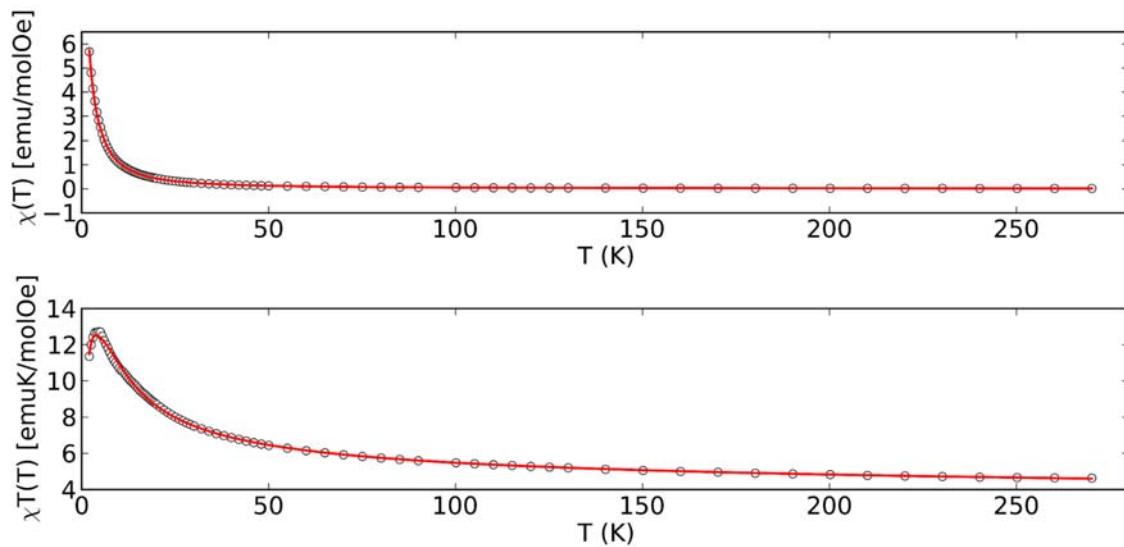


Figure 20: $\chi(T)$ and $\chi T(T)$ dependences for **7**. Red line represents best-fitted curve.

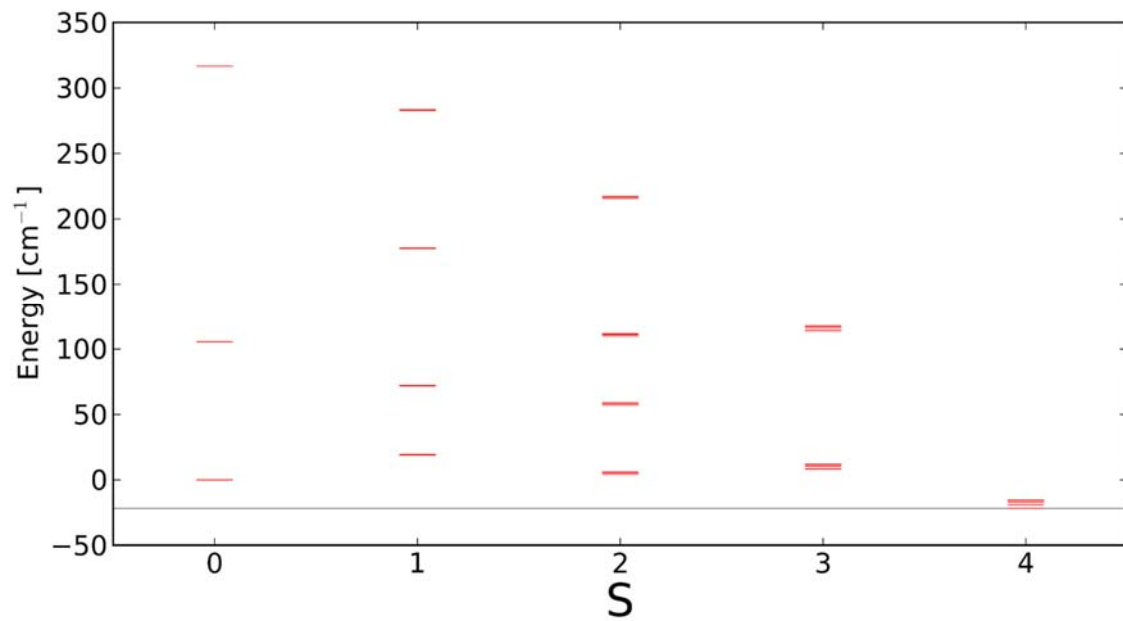


Figure S21: Energy levels diagram for **7**.

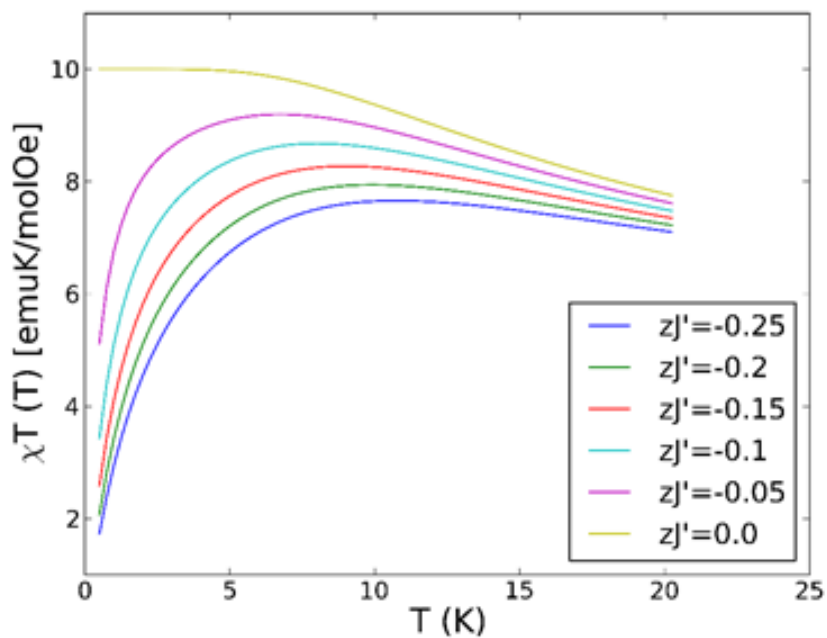


Figure S22. Simulation of contribution of intermolecular interactions to the χT

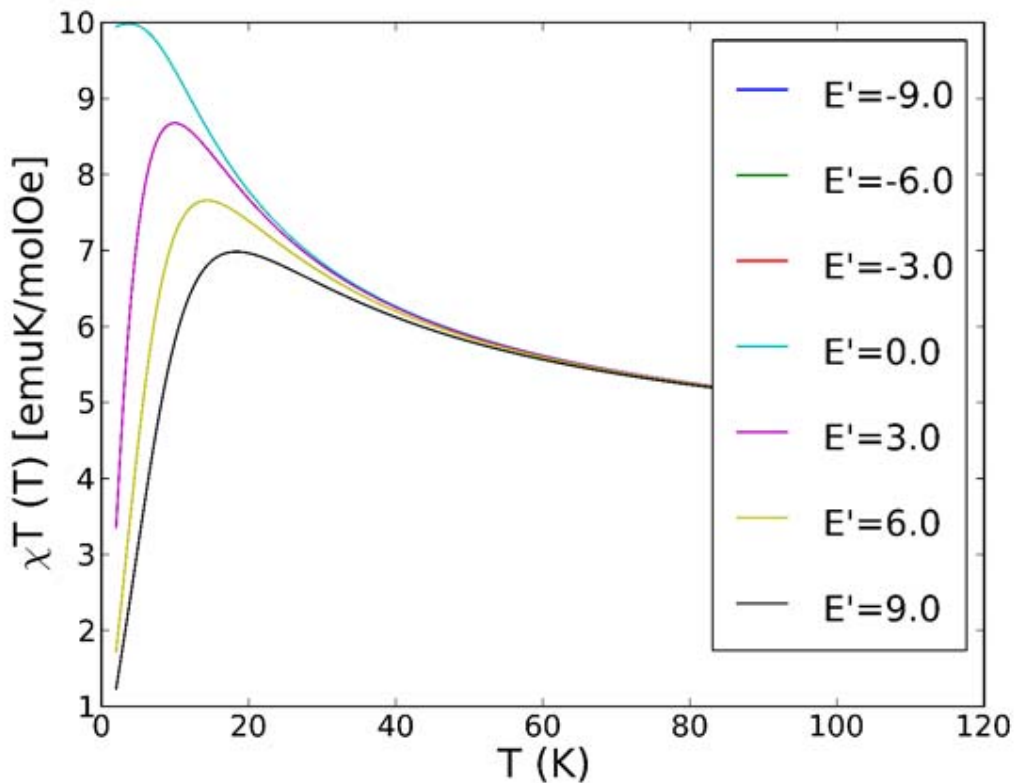


Figure S23. Simulation of contribution of the rhombic E ZFS parameter to the χT .

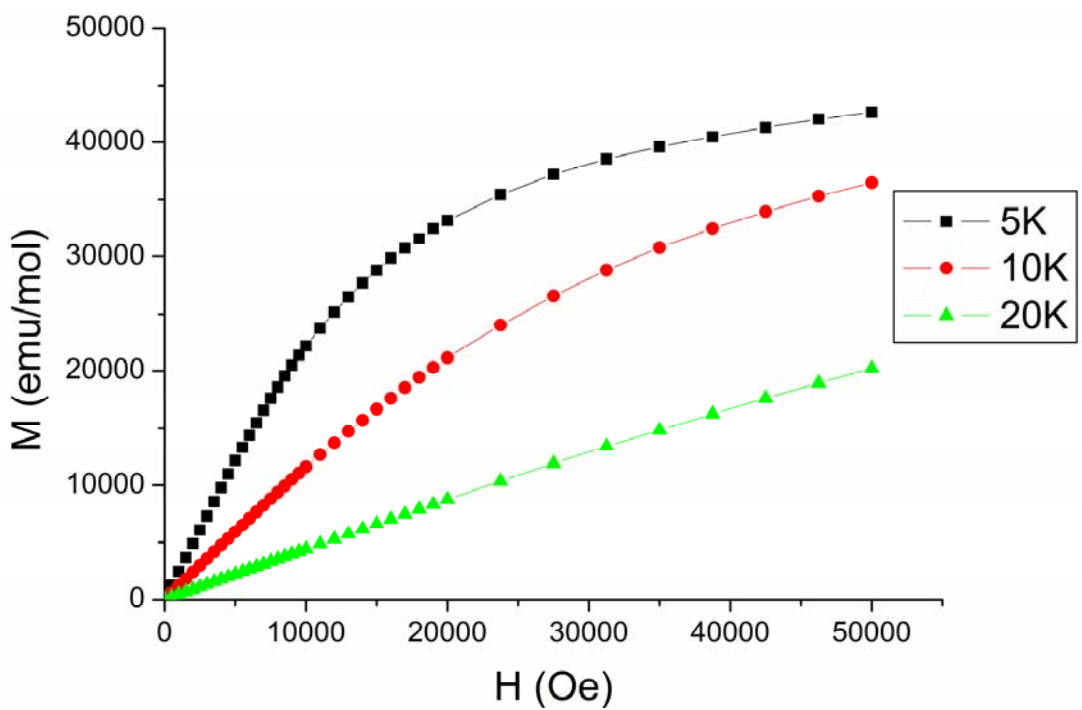


Figure S24: $M(H)$ curves for **1** measured at several temperatures

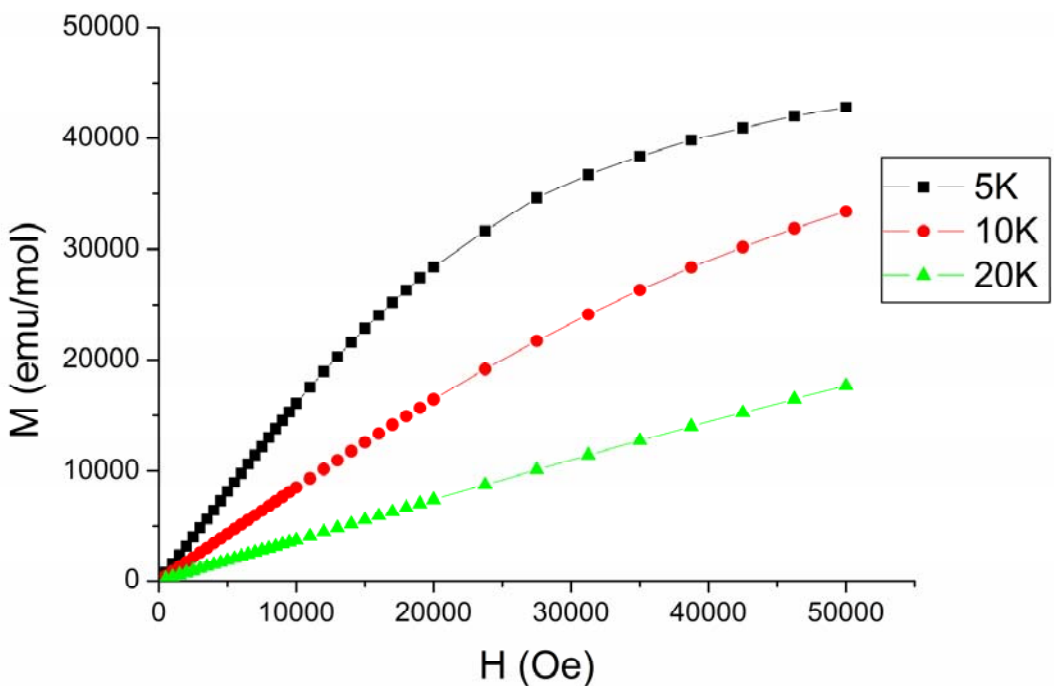


Figure S25: $M(H)$ curves for **2** measured at several temperatures

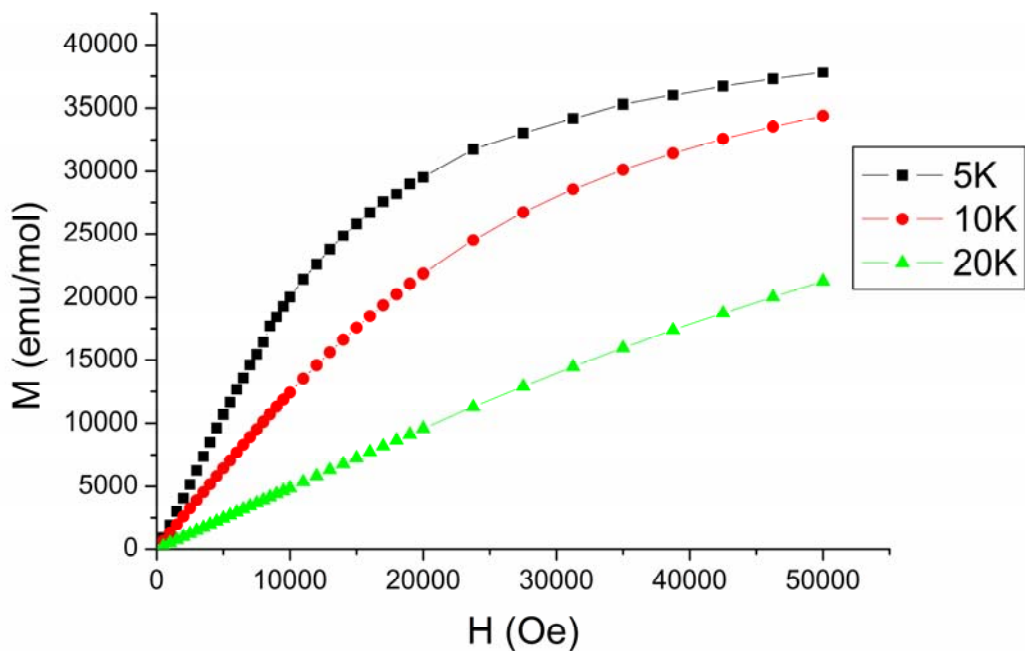


Figure S26: $M(H)$ curves for **3** measured at several temperatures

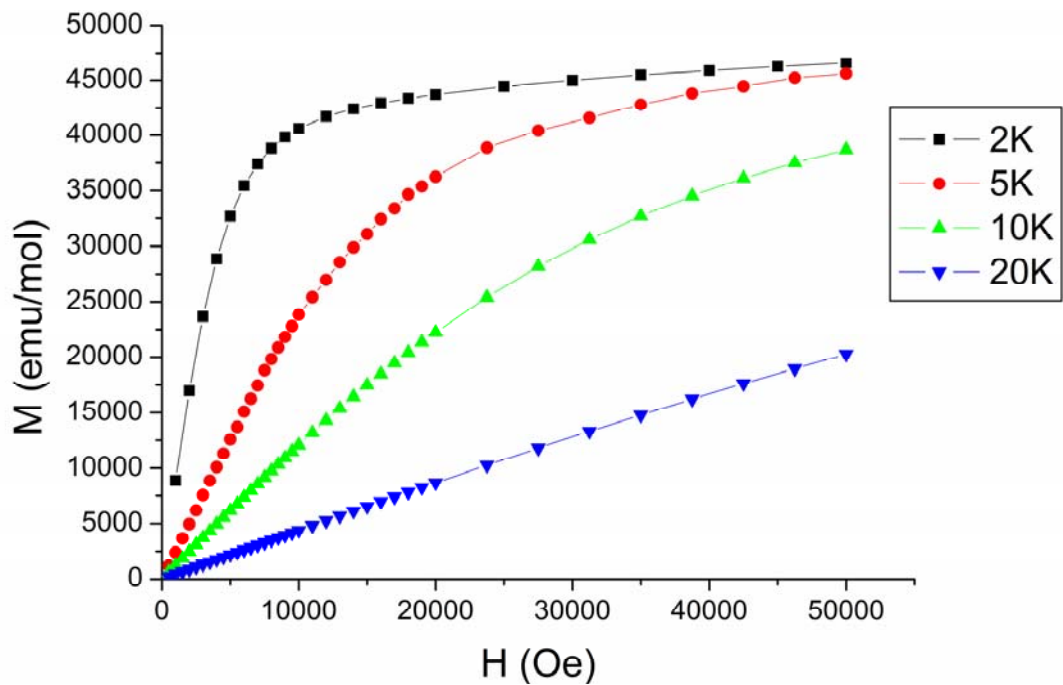


Figure S27: $M(H)$ curves for **4** measured at several temperatures

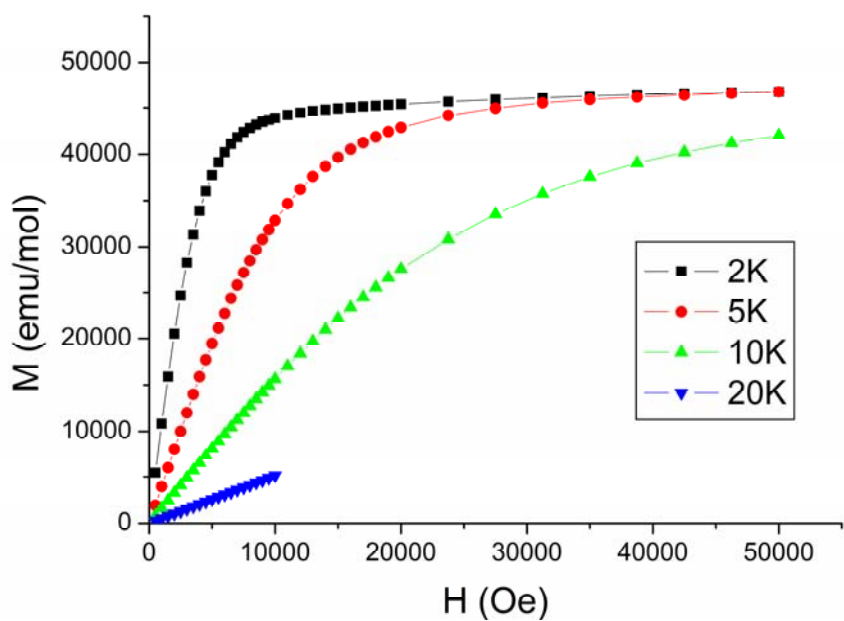


Figure S28: $M(H)$ curves for **5** measured at several temperatures

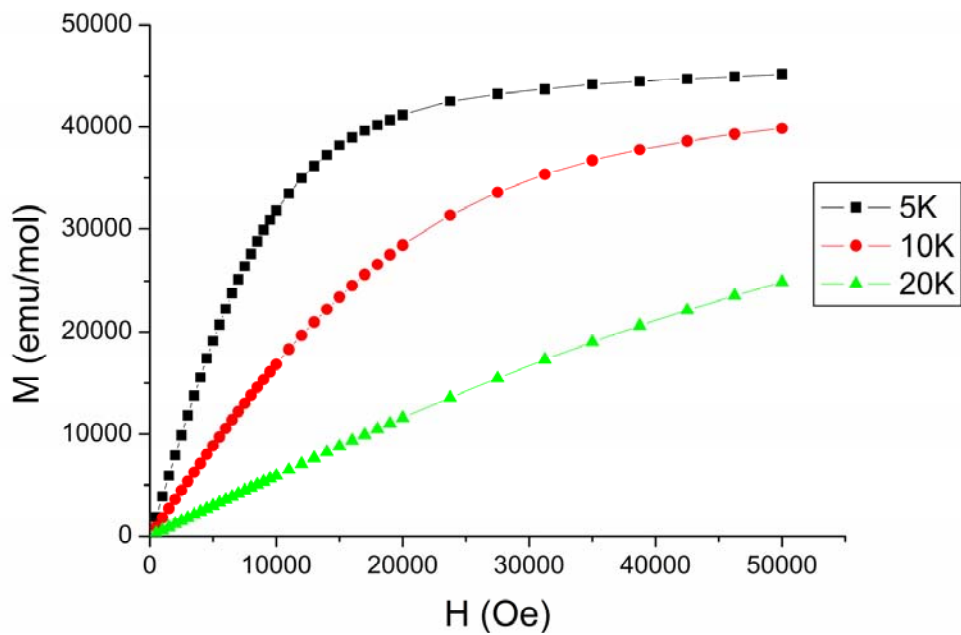


Figure S29: $M(H)$ curves for **6** measured at several temperatures

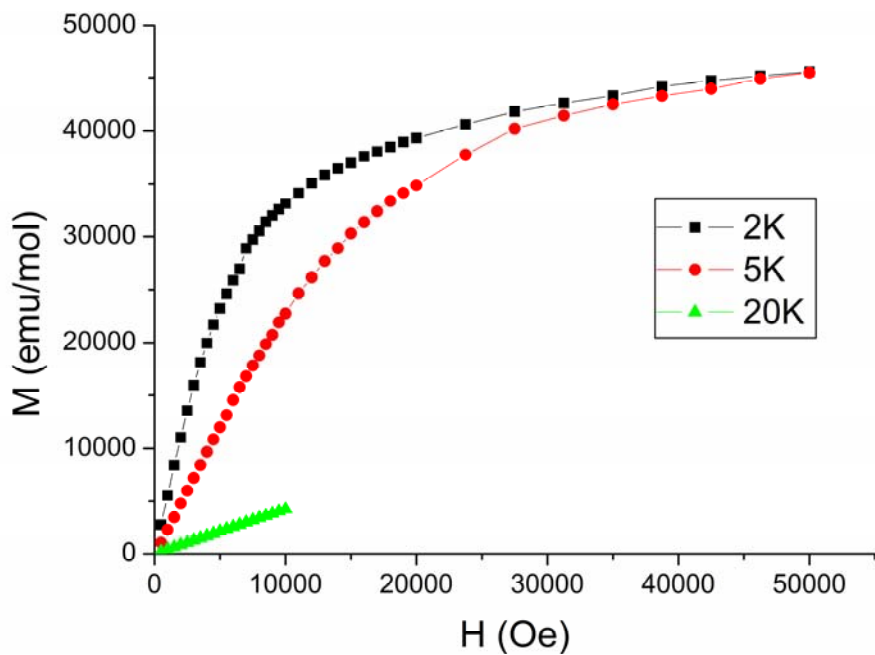


Figure S30: $M(H)$ curves for **7** measured at several temperatures

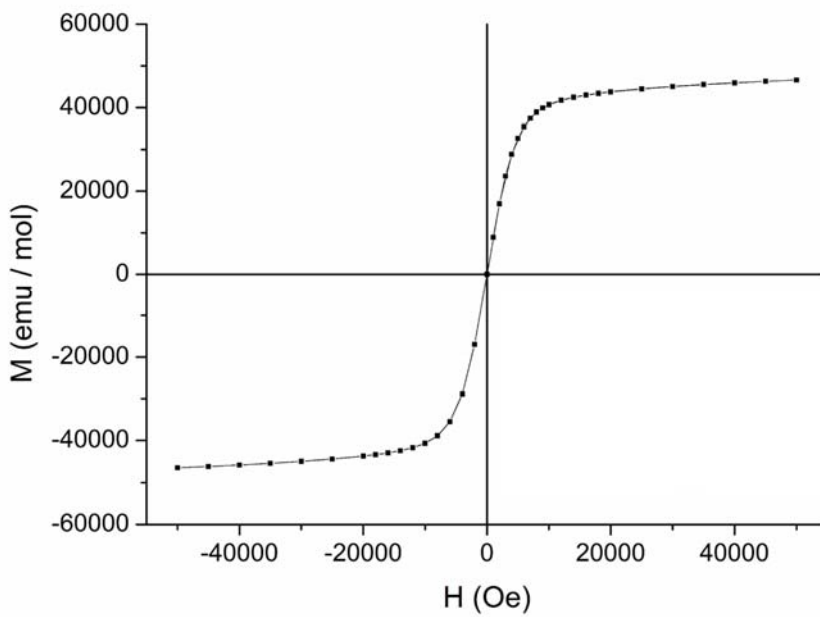


Figure S31: Hysteresis curve for **4** measured at 2K.

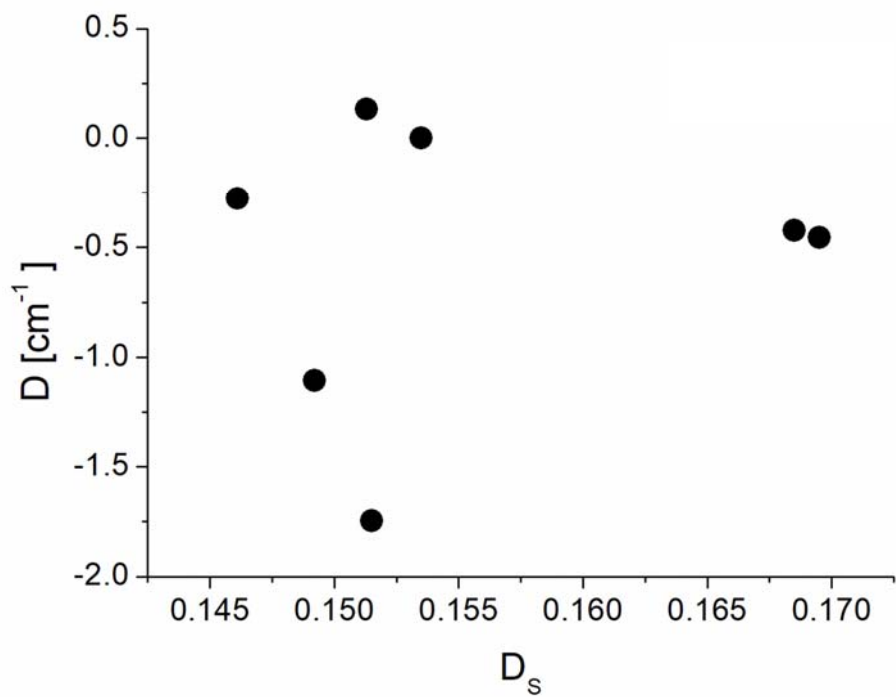


Figure S32: Dependence of zero-field splitting D to D_s defined in text.

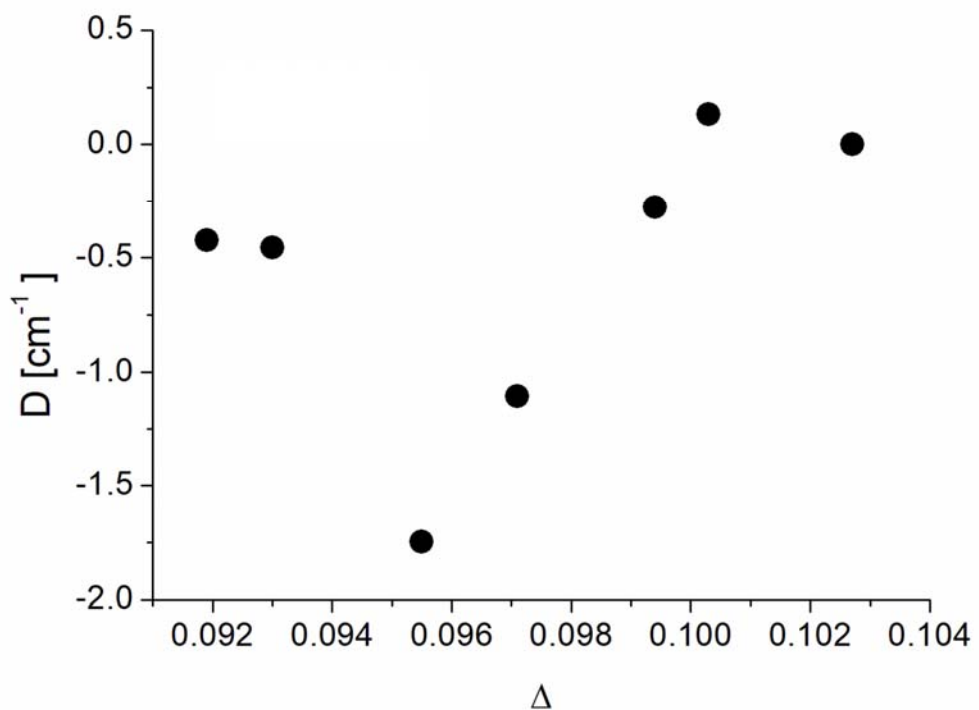


Figure S33: Dependence of zero-field splitting D to the average difference between longer and shorter bonds in the Ni octahedra.

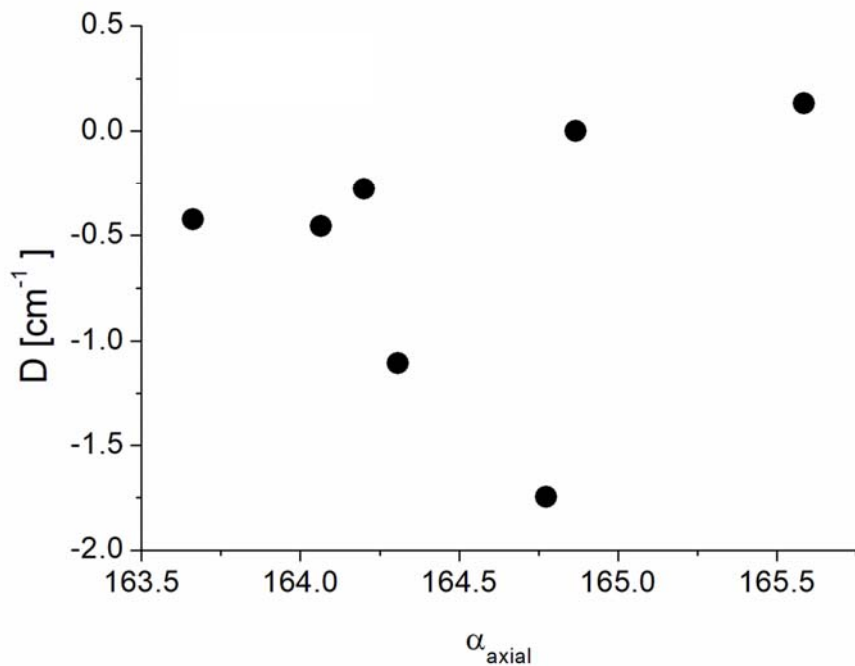


Figure S34: Dependence of zero-field splitting D to the axial angle α_{axial} .